Geological Society of America Bulletin

Sediment production and delivery in the Amazon River basin quantified by in situ –produced cosmogenic nuclides and recent river loads

Hella Wittmann, Friedhelm von Blanckenburg, Laurence Maurice, Jean-Loup Guyot, Naziano Filizola and Peter W. Kubik

Geological Society of America Bulletin 2011;123, no. 5-6;934-950
doi: 10.1130/B30317.1

Notes

Sediment production and delivery in the Amazon River basin quantified by in situ–produced cosmogenic nuclides and recent river loads

Hella Wittmann[1,*,†], Friedhelm von Blanckenburg[1,*], Laurence Maurice[2,3], Jean-Loup Guyot[4], Naziano Filizola[5], and Peter W. Kubik[6]

[1]*Institut für Mineralogie, Universität Hannover, Callinstrasse 3, 30167 Hannover, Germany*
[2]*Université de Toulouse, Université Paul Sabatier (UPS), Observatoire Midi-Pyrénées (OMP) and Laboratoire Mécanismes et Transferts en Géologie (LMTG), 14 Av. E. Belin, 31400 Toulouse, France*
[3]*Institut de recherche pour le développement (IRD), Laboratoire Mécanismes et Transferts en Géologie (LMTG), 14 Av. E. Belin, 31400 Toulouse, France*
[4]*Instituto de Pesquisa para o Desenvolvimento (Institut de recherche pour le développement [IRD]), CP 7091 Lago Sul, 71619-970 Brasília, Brazil*
[5]*The Federal University of Amazonas, Av. Darcy Vargas, 1200 s/C-28, 69050-020 Manaus, Brazil*
[6]*Laboratory of Ion Beam Physics, Eidgenössische Technische Hochschule Zürich (ETH), 8093 Zürich, Switzerland*

ABSTRACT

We use cosmogenic nuclide-derived denudation rates from in situ–produced ^{10}Be in river sediment to determine sediment production rates for the central Amazon River and its major tributaries. Recent developments have shown that this method allows calculating denudation rates in large depositional basins despite intermediate sediment storage, with the result that fluxes of the sediment-producing hinterland can now be linked to those discharged at the basins' outlet. In rivers of the central Amazonian plain, sediment of finer grain sizes (125–500 µm) yields a weighted cosmogenic nuclide-derived denudation rate of 0.24 ± 0.02 mm/yr that is comparable to the integrated rate of all main Andean-draining rivers (0.37 ± 0.06 mm/yr), which are the Beni, Napo, Mamoré, Ucayali, and Marañón rivers. Coarser-grained sediment (>500 µm) of central Amazonian rivers is indicative of a source from the tectonically stable cratonic headwaters of the Guyana and Brazilian shields, for which the denudation rate is 0.01–0.02 mm/yr. Respective sediment loads can be calculated by converting these cosmogenic nuclide-derived rates using their sediment-producing areas. For the Amazon River at Óbidos, a sediment production rate of ~610 Mt/yr results; non-Andean source areas contribute only ~45 Mt/yr. A comparison with published modern sediment fluxes shows similarities within a factor of ~2 with an average gauging-derived sediment load of ~1000 Mt/yr at Óbidos, for example. We attribute this similar trend in cosmogenic versus modern sediment loads first to the absence of long-term deposition within the basin and second to the buffering capability of the large Amazon floodplain. The buffering capability dampens short-term, high-amplitude fluctuations (climatic variability in source areas and anthropogenic soil erosion) by the time the denudation rate signal of the hinterland is transmitted to the outlet of the basin.

INTRODUCTION

The Amazon River is the world's largest fluvial system in terms of water discharge and drainage area, and presently exports a total sediment load of ~550–1500 Mt/yr to the Atlantic Ocean (e.g., Meade et al., 1979; Gaillardet et al., 1997; Dunne et al., 1998; Guyot et al., 2005; Martinez et al., 2009). Based on modern sediment load measurements, it has been suggested that the export of sediment does not correspond to the total sediment flux discharged from the Andes and cratonic shields. Guyot et al. (1993) estimated that currently roughly 40% of Andean sediment flux is intercepted and deposited in the basins close to the foothills of the Bolivian Andes. Consequently, it is reasonable to expect that most sediment passing Óbidos has resided in the floodplain for some time since its initial denudation in the Andes. The question is whether this storage is temporary, and whether the deposition of sediment detected from modern loads represents a long-term process. Storage times have been estimated for the present Amazon River configuration to be on the order of several thousand years, ranging from ~5 k.y. on the basis of sediment budgets (Mertes et al., 1996; Mertes and Dunne, 2007), to ~14 k.y. from U-series constraints (Dosseto et al., 2006a; Dosseto et al., 2006b). Storage of sediment for unknown durations potentially compromises erosion rate estimates from gauging (Walling, 1983), so that an increasing need arises for a method that can estimate sediment production by erosion while being insensitive to storage effects in floodplains. In situ–produced cosmogenic isotopes (^{10}Be and ^{26}Al) are routinely measured in quartz from river sediment for estimating denudation rates in steady-state hill-slope settings over time scales relevant to soil formation processes (e.g., Bierman and Steig, 1996; Granger et al., 1996; Schaller et al., 2001; von Blanckenburg, 2005; Granger and Riebe, 2007). In a recent extension to the method, Wittmann and von Blanckenburg (2009) modeled the effect of floodplain sediment storage on cosmogenic nuclide-derived denudation rates. These authors showed that nuclide concentrations accumulated in source areas are under most conditions conserved if storage times are a few thousand years. Hence, cosmogenic nuclide-derived denudation rates can provide a measure of sediment production at the same time scale. Wittmann et al. (2009) tested this approach in large Amazon tributaries, the Beni and Mamoré basins, where the average Andean denudation rate is preserved throughout several hundreds of kilometers of floodplain storage.

*Present address: GeoForschungsZentrum Potsdam, Telegrafenberg, 14473 Potsdam, Germany
†E-mail: wittmann@gfz-potsdam.de

GSA Bulletin; May/June 2011; v. 123; no. 5/6; p. 934–950; doi: 10.1130/B30317.1; 7 figures; 3 tables; Data Repository item 2011019.

In the present study, we directly compare apparent sediment loads calculated from cosmogenic nuclide-derived denudation rates (Table 1) to those derived from modern sediment flux measurements in central Amazonian rivers. Our construction of a sediment mass budget for the Amazon trunk stream, the major tributaries, the Andean source areas, and the cratonic shields serves to evaluate the capability of large floodplains to buffer sediment export against human-induced and climatic changes.

STUDY AREA

The trunk stream of the Amazon River in Brazil is formed by three main tributaries, which are the Solimões, draining the central Andes, the Negro River draining the Guyana Shield, and the Madeira River, a mixed load river draining the Bolivian and Peruvian Andes and the Brazilian Shield (see Fig. 1). In Peru, the Solimões is also called "Amazonas." The Andes comprise only 11% of the total Amazon basin area, but are thought to contribute ~90% of the total suspended load carried by the Amazon River at Óbidos (Meade et al., 1985). The Brazilian Shield to the south and the Guyana Shield to the north of the Amazon valley, respectively, are highly weathered cratonic areas that consist of granitic Precambrian basement of mostly Proterozoic age (Hartmann and Delgado, 2001; Mertes and Dunne, 2007), but these areas are thought to contribute only minor amounts of sediment (Filizola and Guyot, 2009). The architecture of the Amazon basin is composed of two distinct settings, with the deforming foreland basins to the northwest and southwest (drained mainly by the Solimões and the Madeira tributaries, respectively), and subsiding central Amazonia with elevations below 200 m (Caputo, 1991; Irion et al., 1995).

Sediment Transport, Sediment Grain Sizes, and Sediment Provenance

The majority of sediment that is transported in the modern channel of the lower Amazon is carried in suspension; bedload transport only accounts for about ~1% of the total sediment load (Strasser, 2002; Guyot et al., 2005). Grain sizes of the Amazon bedload range between 0.1 and 1 mm with estimates of median sizes ranging from 0.26 to 0.38 mm for the reach between Iquitos and the Amazon mouth (Nordin et al., 1980; Franzinelli and Potter, 1983). Mertes and Meade (1985) report a median size of 0.25 mm for the reach between Vargem Grande (at Rio Içа confluence) and Óbidos, and also note that the overall cross-channel variability in particle size is much greater due to hydraulic sorting in bends than the slight effect of downstream fining observed (Mertes and Meade, 1985). Near-absence of downstream fining in the Amazon basin is an effect also observed, e.g., in the Beni River (Guyot et al., 1999). Mitigation of downstream fining in the Amazon River is the result of the addition of coarser sediment from Brazilian and Guyana shield weathering (Nordin et al., 1980; Franzinelli and Potter, 1983). Material derived from cratonic shields has a median size of 0.42 mm according to Franzinelli and Potter (1983) (see their fig. 5). This sediment addition from highly weathered terrains is accompanied with a change in mineral composition; Andean-derived bedload contains more rock fragments and feldspar than quartz-rich sands from Precambrian-dominated cratonic watersheds (Franzinelli and Potter, 1983). In general, high maturity indices for heavy minerals reflect the intensely weathered areas of the cratonic shields and their overlying Cretaceous and Tertiary products (e.g., Alter do Chão and Barreiras, and Post-Barreiras formations), whereas Andean-derived sediment is less mature (Vital et al., 1999). Indicative of their source areas are also clay mineral assemblages: illite and chlorite dominate Andean-derived sediment, kaolinite is mostly present in Guyana and Brazilian shield sediments, and sediment of the Amazon lowlands is enriched in smectite (Vital et al., 1999; Guyot et al., 2007b). This smectite enrichment across the floodplain has been interpreted as an increase in the relative proportion of bank sediment admixed to mainstream mostly Andean-derived sediment from lateral bank erosion (Johnsson and Meade, 1990; Guyot et al., 2007b).

Published Modern Sediment Loads

For major rivers of the Amazon basin, suspended load values from gauging stations were compiled from several different sources (Meade, 1985; Guyot et al., 1996; Dunne et al., 1998; Guyot et al., 1999; Maurice-Bourgoin et al., 2002; Filizola, 2003; Moreira-Turcq et al., 2003; Seyler and Boaventura, 2003; Guyot et al., 2005; Laraque et al., 2005; Guyot et al., 2007a; Filizola and Guyot, 2009; Laraque et al., 2009; Martinez et al., 2009); where more than one published suspended sediment value was available, we selected the lowest and the highest values (see Table 2). Guyot et al. (1996) measured dissolved loads for gauging stations located in Bolivia over the same time interval as their suspended load equivalents, so that in these cases a direct comparison between suspended and dissolved loads is feasible. Dissolved loads for other gauging stations (see Table 2) were measured by Gaillardet et al. (1997) during a sampling cruise in May 1989. In the following, the sum of dissolved and suspended loads will be called "modern total load" (Q_M). It is important to note that cosmogenic nuclide-derived denudation rates detect total, e.g., physical and chemical denudation (e.g., von Blanckenburg, 2005). Therefore, for modern loads, we use both suspended and dissolved fluxes throughout.

We assigned an average method-associated uncertainty of 20% on modern loads. In cases where, e.g., depth-integrated sampling was carried out (e.g., Filizola, 2003; Guyot et al., 2005; Martinez et al., 2009), this uncertainty probably is justified, but for studies where a depth-integration of suspended particulate matter (SPM) concentrations is absent, the uncertainty is probably an underestimation, because the depth-distribution of SPM concentrations is almost certainly not homogenous (Filizola, 2003). However, we expect that the natural variability of sediment discharge not contained in the gauging period is much larger than the method-associated error. This potential bias will be explored in "Comparison between cosmogenic nuclide-derived and modern sediment loads."

METHODS

Our sampling strategy is described in GSA Data Repository Appendix DR1[1], and sampling locations are given in Table 1. All samples were taken during cruises operated by the HYBAM project, a collaboration of the French Institut de recherche pour le développement Institute with South American institutes and universities. Samples were dried, sieved into narrow grain-size ranges, and pure quartz was separated using magnetic separation followed by etching with weak HF. We used the simplified method of von Blanckenburg et al. (2004) to separate in situ–produced ^{10}Be from the sample matrix. The ^{9}Be carrier added to each sample was determined to contain a ^{10}Be/^{9}Be ratio of $1.25 \pm 0.41 \times 10^{-14}$, except samples denoted by a footnote in Table 1. After Be purification, samples were oxidized and pressed into accelerator mass spectrometer (AMS) cathodes and were measured at the Eidgenössische Technische Hochschule Zürich AMS facility (Synal et al., 1997). Production rate calculation (using pixel-based altitudes derived from 1 km resolution Shuttle Radar Topographic Mission–digital elevation model), atmospheric scaling, and calculation of absorption laws were identical to those of previous studies (Wittmann et al., 2007; Wittmann et al., 2009).

[1]GSA Data Repository item 2011019, Data Repository item contains information on sampling strategy, AMS standardization, and details on nuclide concentrations and denudation rate calculations, is available at http://www.geosociety.org/pubs/ft2011.htm or by request to editing@geosociety.org.

TABLE 1. BASIN AND SAMPLE CHARACTERISTICS AND ANALYTICAL RESULTS

Sample[a]	River and setting	Note[b]	Basin area ($\times 10^4$ km^2)	Basin average mean altitude (m)	Grain size (μm)	Sample weight (g)	^{10}Be concentration[c] ($\times 10^4$ ats/g$_{(Qz)}$)	^{26}Al/^{10}Be ratio[d]	^{10}Be production rate[e] (ats/g$_{(Qz)}$/yr)	Denudation rate[f] (mm/yr)	^{10}Be production rate corrected for area[g] (ats/g$_{(Qz)}$/yr)	Floodplain-corrected denudation rate[h] (mm/yr)	Apparent age[i] (kyr)	Samples used for denudation calculation in Table 3
Andean tributary samples: Ucayali and Solimões (IDs 1 and 2 in Table 3 and all figures)														
Pe 107a-1[j]	Ucayali at Requena		36.0	1713	125–250	58.8	5.64 ± 0.63	-	18.0	0.25 ± 0.03	24.0	0.32 ± 0.04	2.3	Yes
Pe 107a-2	-″-		-″-	-″-	-″-	32.0	5.03 ± 0.39	6.82 ± 1.58	18.0	0.28 ± 0.03	24.0	0.36 ± 0.03	2.1	Yes
Pe 101a-1[j]	Solimões at Tamshiyacu		73.3	1432	125–250	50.4	7.30 ± 0.51	-	14.3	0.15 ± 0.01	16.8	0.21 ± 0.02	4.4	Yes
Pe 101a-2	–″–		-″-	-″-	-″-	19.3	8.04 ± 0.85	6.13 ± 0.97	14.3	0.14 ± 0.02	16.8	0.19 ± 0.02	4.8	Yes
Guyana Shield samples: Branco River (profile along river; ID 6 in Table 3 and all figures)														
Br 1a[k]	Branco		14.6	397	125–250	34.7	35.10 ± 1.56	6.16 ± 0.51	5.2	0.0120 ± 0.0008	5.9	0.0138 ± 0.0010	60.1	Yes
Br 2a[k]	-″-		14.7	397	125–250	44.6	45.13 ± 1.62	-	5.2	0.0091 ± 0.0008	5.9	0.0104 ± 0.0009	77.5	No
Br 2b[k]	-″-		-″-	-″-	250–500	31.1	46.82 ± 3.38	-	5.2	0.0087 ± 0.0006	5.9	0.0100 ± 0.0007	80.5	No
Br 4b[k]	-″-		15.1	386	250–500	25.2	44.69 ± 2.07	-	5.2	0.0091 ± 0.0006	6.0	0.0106 ± 0.0008	76.4	No
Br 4c[k]	-″-		-″-	-″-	500–800	35.1	31.99 ± 1.55	5.80 ± 0.59	5.2	0.0132 ± 0.0009	6.0	0.0153 ± 0.0011	54.4	No
Br 5b[k]	-″-		17.5	358	250–500	9.0	46.91 ± 3.95	3.91 ± 0.49	5.1	0.0084 ± 0.0008	5.8	0.0098 ± 0.0010	81.8	No
Br 5c[k]	-″-		-″-	-″-	500–800	54.6	33.87 ± 2.22	5.60 ± 0.51	5.1	0.0121 ± 0.0010	5.8	0.0141 ± 0.0012	58.8	No
Br 6a[k]	-″-		21.3	329	125–250	50.3	43.95 ± 3.92	-	5.0	0.0088 ± 0.0009	5.8	0.0106 ± 0.0011	76.5	No
Br 6b[k]	-″-		-″-	-″-	250–500	48.8	35.53 ± 2.29	-	5.0	0.0112 ± 0.0010	5.8	0.0134 ± 0.0011	61.6	No
Br 8a[k]	-″-		21.0	332	250–250	23.4	43.49 ± 3.09	-	5.0	0.0089 ± 0.0008	5.8	0.0107 ± 0.0009	75.7	No
Br 8b-1[k]	-″-		-″-	-″-	250–500	61.9	32.24 ± 2.78	-	5.0	0.0125 ± 0.0013	5.8	0.0149 ± 0.0015	55.8	No
Br 8b-2	-″-		-″-	-″-	-″-	16.6	32.20 ± 2.10	5.27 ± 0.51	5.0	0.0125 ± 0.0013	5.8	0.0149 ± 0.0015	55.8	No
Brazilian Shield: Upper Madeira River tributaries (ID 14 in Table 3 and all figures)														
Cb 1a[l]	Guaporé at Pontes e Lacerda		0.7	449	160–250	50.2	23.18 ± 1.12	-	5.8	0.021 ± 0.001	-	-	40.4	Yes
Cb 2a	Guaporé at Pimenteiras		11.0	350	125–250	28.2	16.16 ± 0.87	6.30 ± 0.55	5.1	0.027 ± 0.003	-	-	31.8	Yes
Cb 3a-1[k]	Aripuana at Aripuana		2.0	260	125–250	41.2	31.25 ± 1.57	-	4.7	0.012 ± 0.001	-	-	67.1	No
Cb 3a-2	-″-		-″-	-″-	-″-	32.1	37.79 ± 3.97	4.89 ± 0.64	4.7	0.010 ± 0.001	-	-	81.4	No
Brazilian Shield: Upper Tapajós River tributaries (ID 19 in Table 3 and all figures)														
Cb 4a-1	Juruena at Juruena		17.7	403	125–250	20.3	11.75 ± 1.07	6.68 ± 0.89	4.9	0.036 ± 0.003	-	-	24.4	Yes
Cb 4a-2[j]	-″-		-″-	-″-	-″-	51.2	13.64 ± 1.59	-	4.9	0.031 ± 0.004	-	-	28.3	Yes
Cb 4a-3[j]	-″-		-″-	-″-	-″-	45.8	15.54 ± 1.43	-	4.9	0.027 ± 0.009	-	-	32.3	Yes
Cb 5b[k]	Apiacás		1.2	298	250–500	61.1	26.76 ± 0.95	-	4.9	0.015 ± 0.001	-	-	55.2	No
Cb 6b-1[k]	Teles Pires Near Rochedo		9.4	371	250–500	64.5	19.00 ± 1.20	-	5.3	0.024 ± 0.002	-	-	36.0	Yes
Cb 6b-2[k]	-″-		-″-	-″-	-″-	55.1	18.05 ± 1.23	-	5.3	0.025 ± 0.002	-	-	34.2	Yes
Cb 6b-3	-″-		-″-	-″-	-″-	37.2	17.50 ± 0.95	5.67 ± 0.58	5.3	0.026 ± 0.003	-	-	33.1	Yes
Cb 7a[l]	Teles Pires at Peixoto Azevedo		1.6	363	125–250	55.1	41.93 ± 3.88	-	5.1	0.010 ± 0.001	-	-	83.9	No
Cb 7b-1[j]	-″-		-″-	-″-	250–500	40.2	39.95 ± 2.33	-	5.1	0.010 ± 0.001	-	-	79.9	No
Cb 7b-2[k]	-″-		-″-	-″-	-″-	11.9	32.90 ± 4.04	5.01 ± 0.76	5.1	0.013 ± 0.002	-	-	65.6	No

(*continued*)

TABLE 1. BASIN AND SAMPLE CHARACTERISTICS AND ANALYTICAL RESULTS (*continued*)

Sample[a]	River and setting	Note[b]	Basin area ($\times 10^4$ km^2)	Basin average mean altitude (m)	Grain size (μm)	Sample weight (g)	^{10}Be concentration[c] ($\times 10^4$ ats/g$_{(Qz)}$)	^{26}Al/^{10}Be ratio[d]	^{10}Be production rate[e] (ats/g$_{(Qz)}$/yr)	Denudation rate[f] (mm/yr)	^{10}Be production rate corrected for area[g] (ats/g$_{(Qz)}$/yr)	Floodplain-corrected denudation rate[h] (mm/yr)	Apparent age[i] (kyr)	Samples used for denudation calculation in Table 3
Xingu River and Brazilian Highland samples (rivers do not drain into Amazon basin at Óbidos)														
Cb 8a[j]	Xingu near Sao José do Xingu		16.9	346	125–250	68.3	25.45 ± 1.89	-	5.1	0.016 ± 0.002	-	-	51.0	No
Cb 8b-1[j]	-"-		-"-	-"-	250–500	72.4	23.24 ± 1.91	-	5.1	0.018 ± 0.002	-	-	46.5	No
Cb 8b-2	-"-		-"-	-"-	-"-	36.5	22.45 ± 0.96	5.11 ± 0.35	5.1	0.019 ± 0.002	-	-	44.9	No
Cb 10a[j]	Brazilian Highlands, Araguaia		10.2	524	125–250	49.4	17.37 ± 0.96	-	5.3	0.026 ± 0.002	-	-	32.9	No
Cb 10b-1[j]	-"-		-"-	-"-	250–500	62.9	11.86 ± 1.08	-	5.3	0.040 ± 0.004	-	-	22.4	No
Cb 10b-2[k]	-"-		-"-	-"-	250–500	16.6	12.23 ± 0.90	5.98 ± 0.86	5.3	0.038 ± 0.007	-	-	23.1	No
Amazon lowland samples ("Llanos") from various rivers (IDs 4, 5, 7, 8, 15, 16, and 18 in Table 3 and all figures)														
Ne Rb-a[k]	Negro near Paricatuba	Right bank	83.2	225	125–250	98.3	10.28 ± 0.47	4.64 ± 0.39	3.9	0.038 ± 0.003	5.4	0.050 ± 0.003	18.9	No
Ne Rb-b[k]	-"-	-"-	-"-	-"-	250–500	59.5	9.14 ± 0.57	5.20 ± 0.48	3.9	0.043 ± 0.003	5.4	0.056 ± 0.005	16.8	No
Ne Rb-c	-"-	-"-	-"-	-"-	500–800	77.6	6.16 ± 0.47	-	3.9	0.066 ± 0.006	5.4	0.085 ± 0.008	11.3	No
Ne Lb-a[k]	-"-	Left bank	-"-	225	125–250	78.4	8.05 ± 0.65	4.04 ± 0.46	3.9	0.050 ± 0.005	5.4	0.064 ± 0.006	14.8	No
Ne Lb-b[k]	-"-	-"-	-"-	-"-	250–500	101.2	7.45 ± 0.39	4.31 ± 0.41	3.9	0.054 ± 0.004	5.4	0.070 ± 0.005	13.7	No
Ne Lb-c	-"-	-"-	-"-	-"-	500–800	44.6	5.54 ± 0.56	-	3.9	0.073 ± 0.008	5.4	0.095 ± 0.011	10.2	No
Man 0.2a	Solimões at Manacapuru	0.2 km flb	227.0	592	125–250	77.8	6.37 ± 0.40	8.47 ± 3.27	7.1	0.099 ± 0.008	16.6	0.243 ± 0.019	3.8	Yes
Man 0.2b	-"-	0.2 km flb	-"-	-"-	250–500	57.5	4.65 ± 0.42	-	7.1	0.136 ± 0.014	16.6	0.334 ± 0.035	2.8	No
Man 0.2c	-"-	-"-	-"-	-"-	500–800	65.4	7.74 ± 0.87	-	7.1	0.081 ± 0.010	16.6	0.199 ± 0.025	4.7	No
Man 1.1a[k]	-"-	1.1 flb	-"-	-"-	125–250	81.6	6.05 ± 0.75	-	7.1	0.104 ± 0.014	16.6	0.255 ± 0.034	3.6	Yes
Man 1.1b	-"-	-"-	-"-	-"-	250–500	80.9	7.60 ± 0.33	4.32 ± 1.17	7.1	0.082 ± 0.006	16.6	0.203 ± 0.013	4.6	No
Man 1.1c-1	-"-	-"-	-"-	-"-	500–800	74.6	7.32 ± 0.52	-	7.1	0.086 ± 0.007	16.6	0.211 ± 0.019	4.4	No
Man 1.1c-2	-"-	-"-	-"-	-"-	-"-	21.5	8.01 ± 0.69	6.00 ± 0.78	7.1	0.078 ± 0.008	16.6	0.192 ± 0.020	4.8	No
Man 2.4a	-"-	2.4 flb	-"-	-"-	125–250	24.1	6.15 ± 0.70	5.43 ± 0.91	7.1	0.102 ± 0.013	16.6	0.251 ± 0.032	3.7	No
Man 2.85a[k]	-"-	2.85 flb	-"-	-"-	125–250	68.1	6.81 ± 0.54	-	7.1	0.092 ± 0.009	16.6	0.226 ± 0.021	4.1	Yes
Man 2.85b[k]	-"-	-"-	-"-	-"-	250–500	73.3	7.30 ± 0.45	-	7.1	0.086 ± 0.007	16.6	0.211 ± 0.017	4.4	No
Ir 0.4b[k]	Amazon at Iracema	0.4 flb	315.4	491	250–500	92.1	8.77 ± 0.56	5.63 ± 1.88	5.9	0.062 ± 0.005	16.6	0.175 ± 0.014	5.3	No
Ir 0.4c[k]	-"-	-"-	-"-	-"-	500–800	98.5	13.31 ± 0.47	6.98 ± 0.67	5.9	0.040 ± 0.003	16.6	0.114 ± 0.007	8.0	No
Ir 1.0b	-"-	1.0 flb	-"-	-"-	250–500	39.3	8.94 ± 0.46	5.27 ± 0.77	5.9	0.061 ± 0.004	16.6	0.172 ± 0.012	5.4	No
Ir 1.0c	-"-	-"-	-"-	-"-	500–800	42.2	14.44 ± 0.72	4.47 ± 0.41	5.9	0.037 ± 0.003	16.6	0.105 ± 0.007	8.7	No
Ir 1.5b[k]	-"-	1.5 flb	-"-	-"-	250–500	99.4	10.10 ± 0.44	3.80 ± 0.82	5.9	0.053 ± 0.004	16.6	0.152 ± 0.010	6.1	No
Ir 1.5c[k]	-"-	-"-	-"-	-"-	500–800	99.0	15.50 ± 0.57	4.67 ± 0.42	5.9	0.034 ± 0.002	16.6	0.098 ± 0.006	9.4	No
Ir 1.75a	-"-	1.75 flb	-"-	-"-	125–250	48.1	6.72 ± 0.55	-	5.9	0.081 ± 0.008	16.6	0.230 ± 0.022	4.1	Yes
Ir 1.75b	-"-	-"-	-"-	-"-	250–500	52.7	6.03 ± 0.62	-	5.9	0.091 ± 0.011	16.6	0.256 ± 0.029	3.6	Yes
Ir 1.75c	-"-	-"-	-"-	-"-	500–800	81.3	12.53 ± 0.73	-	5.9	0.043 ± 0.003	16.6	0.122 ± 0.010	7.6	No
Mad 0.5a	Madeira at Amazon confluence	0.5 flb	143.8	552	125–250	36.2	6.41 ± 0.57	-	5.3	0.079 ± 0.008	12.8	0.185 ± 0.019	5.0	Yes
Mad 0.5b	-"-	-"-	-"-	-"-	250–500	36.9	8.86 ± 0.84	-	5.3	0.057 ± 0.006	12.8	0.133 ± 0.014	6.9	No
Mad 1.1b	-"-	1.1 flb	-"-	-"-	250–500	55.7	11.50 ± 0.95	-	5.3	0.043 ± 0.004	12.8	0.102 ± 0.010	9.0	No
Mad 1.1c	-"-	-"-	-"-	-"-	500–800	69.2	21.80 ± 0.97	4.79 ± 0.52	5.3	0.022 ± 0.001	12.8	0.052 ± 0.003	17.1	No

(*continued*)

TABLE 1. BASIN AND SAMPLE CHARACTERISTICS AND ANALYTICAL RESULTS (*continued*)

Sample[a]	River and setting	Note[b]	Basin area ($\times 10^4$ km^2)	Basin average mean altitude (m)	Grain size (μm)	Sample weight (g)	^{10}Be concentration[c] ($\times 10^4$ ats/g$_{(Qz)}$)	^{26}Al/^{10}Be ratio[d]	^{10}Be production rate[e] (ats/g$_{(Qz)}$/yr)	Denudation rate[f] (mm/yr)	^{10}Be production rate corrected for area[g] (ats/g$_{(Qz)}$/yr)	Floodplain-corrected denudation rate[h] (mm/yr)	Apparent age[i] (kyr)	Samples used for denudation calculation in Table 3
Amazon lowland samples ("Llanos") from various rivers (IDs 4, 5, 7, 8, 15, 16, and 18 in Table 3 and all figures) (*continued*)														
Mad 1.8a[k]	-"-	1.8 flb	-"-	-"-	125–250	42.5	4.70 ± 0.63	-	5.3	0.109 ± 0.016	12.8	0.253 ± 0.037	3.7	Yes
Mad 1.8b[k]	-"-	-"-	-"-	-"-	250–500	87.7	6.56 ± 0.38	6.65 ± 2.51	5.3	0.077 ± 0.006	12.8	0.180 ± 0.014	5.1	Yes
Par 0.9a	Amazon at Parintins	0.9 flb	473.6	498	125–250	53.7	6.20 ± 0.36	5.89 ± 0.75	5.6	0.082 ± 0.006	15.4	0.231 ± 0.018	4.0	Yes
Par 1.2b	-"-	1.2 flb	-"-	-"-	250–500	48.8	9.43 ± 0.71	-	5.6	0.055 ± 0.005	15.4	0.151 ± 0.014	6.1	No
Par 1.2c	-"-	-"-	-"-	-"-	500–800	49.0	16.74 ± 1.78	-	5.6	0.030 ± 0.004	15.4	0.084 ± 0.010	10.9	No
Par 2.2a[k]	-"-	2.2 flb	-"-	-"-	125–250	32.3	6.88 ± 0.80	-	5.6	0.076 ± 0.010	15.4	0.208 ± 0.026	4.5	Yes
Par 2.2b	-"-	-"-	-"-	-"-	250–500	52.6	6.83 ± 0.62	6.45 ± 3.09	5.6	0.077 ± 0.008	15.4	0.196 ± 0.023	4.7	Yes
Ama-a[k]	Amazon near Óbidos		508.8	478	125–250	51.7	7.22 ± 0.65	-	5.7	0.073 ± 0.007	15.4	0.197 ± 0.020	4.7	Yes
Ama-b	-"-		-"-	-"-	250–500	76.6	8.32 ± 0.40	4.16 ± 1.25	5.7	0.063 ± 0.004	15.4	0.171 ± 0.012	5.4	No
Tapa-b-1[k]	Tapajós near Santarem		59.8	288	250–500	126.5	9.65 ± 0.52	-	4.0	0.041 ± 0.003	4.4	0.045 ± 0.003	22.2	No
Tapa-b-2	-"-		-"-	-"-	-"-	33.3	10.54 ± 0.65	6.75 ± 0.59	4.0	0.038 ± 0.003	4.4	0.041 ± 0.003	24.3	No
Tapa-c[k]	-"-		-"-	-"-	500–800	95.7	8.85 ± 0.56	5.71 ± 0.59	4.0	0.045 ± 0.004	4.4	0.049 ± 0.004	20.4	No
Central Amazon floodplain samples ("Varzea do Curuai"; ID 17 in Table 3 and all figures)														
Soc-b	Lago Grande at Villa Soccurru	Lake	0.4	-	250–500	52.0	4.73 ± 0.42	6.05 ± 0.99	4.0	0.088 ± 0.009	15.4	0.304 ± 0.030	3.1	Yes
Soc-c1	-"-	-"-	-"-	-	500–800	89.7	4.73 ± 0.22	6.42 ± 0.95	4.0	0.088 ± 0.006	15.4	0.304 ± 0.021	3.1	Yes
Soc-c2	-"-	-"-	-"-	-	-"-	48.0	4.25 ± 0.41	-	4.0	0.098 ± 0.011	15.4	0.338 ± 0.037	2.8	Yes
Gran-b	Lago Grande at Curuai	Lake	0.4	-	250–500	98.9	6.84 ± 0.41	6.70 ± 0.93	4.0	0.060 ± 0.005	15.4	0.209 ± 0.016	4.4	Yes
Gran-c	-"-	-"-	-"-	-	500–800	100.4	5.45 ± 0.35	6.22 ± 0.77	4.0	0.076 ± 0.006	15.4	0.263 ± 0.022	3.5	Yes
Curu-a	Lago Curumucuri	Lake	0.4	-	125–250	46.2	14.74 ± 0.79	3.42 ± 0.35	4.0	0.026 ± 0.002	-	-	37.6	No
Curu-b[k]	-"-	-"-	-"-	-	250–500	89.6	10.17 ± 0.44	2.80 ± 0.30	4.0	0.039 ± 0.003	-	-	25.9	No

[a]Sample codes are: "a, b, c" for different grain sizes, and "1, 2, 3" are replicate analysis carried out over the course of three years.

[b]The note gives the positions perpendicular to the left bank (in km from left bank "flb"), from which samples were dredged; other samples were taken from the active river bank and/or beach.

[c]1σ uncertainty contains analytical error of accelerator mass spectrometer (AMS) measurement that was carried out relative to standard S555 (nominal value of ^{10}Be/^{9}Be = 95.5 × 10^{-12}) and a ^{10}Be half-life of 1.51 Myr (Hofmann et al., 1987); the ^{10}Be/^{9}Be ratio of the ^{9}Be carrier is 1.25 ± 0.41 × 10^{-14}, except for samples that are denoted with an Arabic numeral in "Sample" column.

[d]A surface ^{26}Al/^{10}Be ratio of 6.5 ± 0.5 (Kubik et al., 1998) is related to AMS standardizations used; a ratio below ~6.5 denotes burial of sample. Corresponding ^{26}Al and ^{27}Al concentrations can be found in Appendix Table DR1 [see footnote 1].

[e]Total basin-wide, pixel-based ^{10}Be production rate from spallogenic and muonic production; in case of Br and Cb samples: corrected for variations in Earth´s magnetic field after Masarik et al. (2001).

[f]Denudation rates with 1σ uncertainties.

[g]Calculated using a sediment-contributing area >200 m in elevation and only integrating over Andean area.

[h]Calculated with floodplain-corrected production rate.

[i]Apparent age is calculated with floodplain-corrected production rate where possible.

[j]^{9}Be carrier added to these samples contains a ratio of ^{10}Be/^{9}Be of 0.55 ± 0.28 × 10^{-14}.

[k]^{9}Be carrier added to these samples contains a ratio of ^{10}Be/^{9}Be of 2.35 ± 1.08 × 10^{-14}.

[l]^{9}Be carrier added to these samples contains a ratio of ^{10}Be/^{9}Be of 1.10 ± 0.66 × 10^{-14}.

Note: -"- —same as.

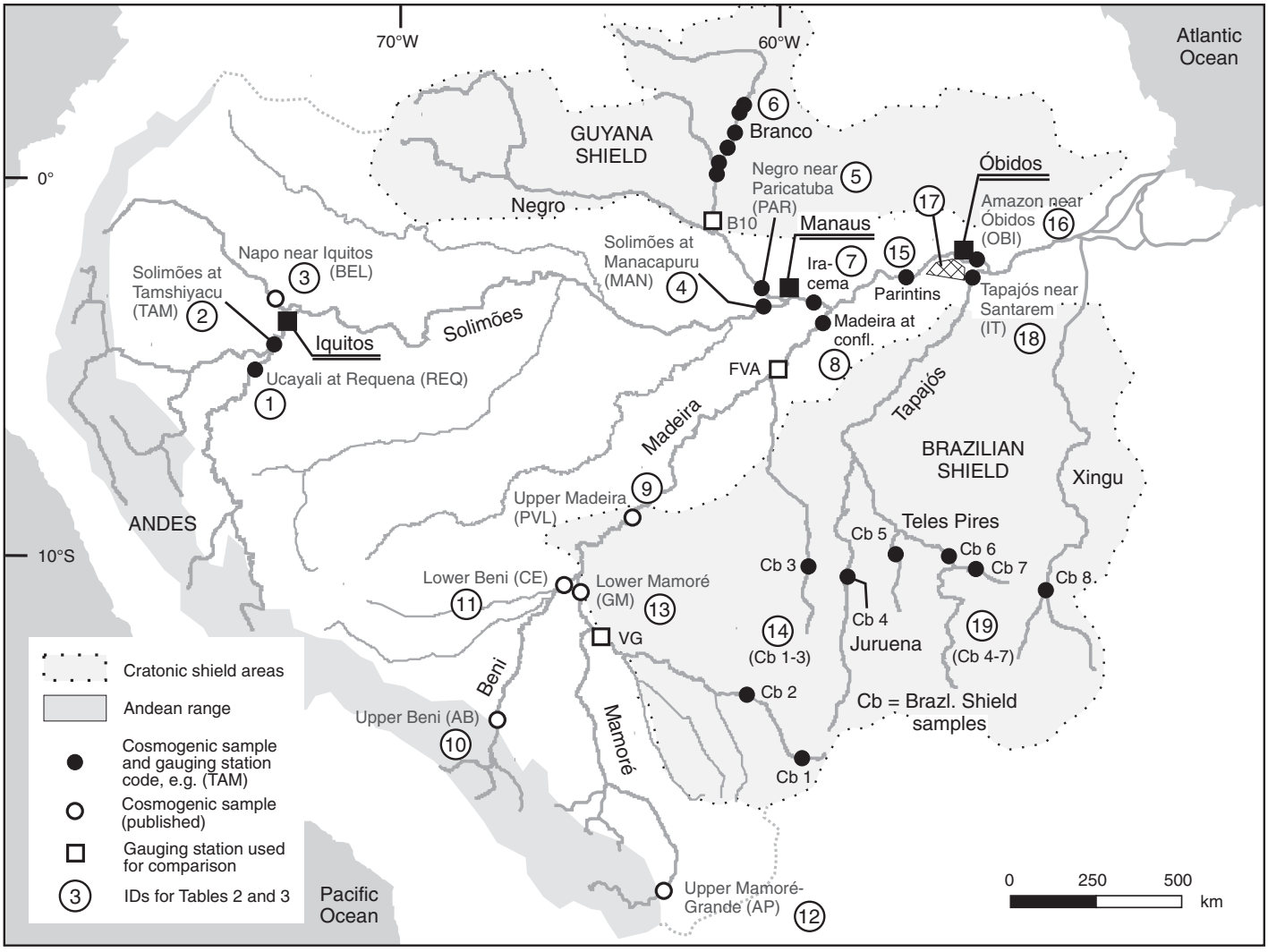

Figure 1. Overview of the Amazon basin and sampling scheme. Circled numbers refer to ^{10}Be nuclide concentrations panels of Figure 3 and to IDs presented in tables.

Sample preparation and inductively coupled–optical emission spectrometer (ICP-OES) measurements of stable aluminum (^{27}Al) were carried out following the procedure described in Goethals et al. (2009) in order to derive ^{26}Al/^{9}Be ratios. Relevant information relating to individual samples can be found in Table 1, and information regarding half-lives and AMS standardization can be found in Appendix DR2 (see footnote 1).

Corrections for variations in the intensity of Earth's magnetic dipole field were carried out following Masarik et al. (2001) for all Brazilian and Guyana shield samples, because these samples integrate over long time scales and are located between 0° and 20°S latitude. Resulting production rate corrections are between 13% and 30%.

We have shown elsewhere (Wittmann and von Blanckenburg, 2009) that under most conditions of floodplains storage, samples conserve the nuclide concentration of their source area. Because in these cases all nuclides have accumulated in the eroding source areas, denudation rates in depositional settings must be calculated using the cosmogenic nuclide production rate of the source area, not of the entire catchment. In Table 1 and Figure 2, we provide this correction, which we call "floodplain-corrected" (see Wittmann et al., 2009, for details on the procedure). Apparent sedimentary loads ("Q_{CN}") were calculated by multiplying these floodplain-corrected, cosmogenic nuclide-derived denudation rates with the sediment-producing area and the sediment density. This allows us to compare our cosmogenic nuclide-based denudation rates with published modern loads.

In the case that storage times approach the half-life of ^{10}Be (i.e., the newly determined value is 1.39 m.y. [Chmeleff et al., 2010]), nuclide concentrations can be modified by both radioactive decay and further production by deep cosmic rays, so that the initial nuclide concentration is not preserved. In the Amazon basin, Tertiary and older formations crop out in distal vicinities of the main modern channel (see detail maps of, e.g., Vital et al., 1999; Rossetti et al., 2005), that are, to some extent, periodically flooded (Martinez and Le Toan, 2007). Sediment stored in basins of the Brazilian and Guyana cratons have been shown to weather on time scales of >300,000 yr (Mathieu et al., 1995; Dosseto et al., 2006a). Therefore, an erosion of these deposits by undercutting of the bank at large channel depths would lead to an incorporation of buried sediments with potentially decayed ^{26}Al/^{10}Be signatures. In separate work currently in preparation, we assess burial depths and durations from our measured ^{26}Al/^{10}Be ratios. In the

TABLE 2. SEDIMENT GAUGING DATA FOR THE UPPER AMAZON TRIBUTARIES AND CENTRAL AMAZON

Gauging station code[a]	Station	River or basin	ID[b]	Total drainage area (×10⁴ km²)	Sediment source area (×10⁴ km²)	Gauging period for suspended loads[c]	Suspended sediment load (range)[d] (Mt/yr)	Specific dissolved load[e] (Mt/yr)	Total yield (range) (t/km²/yr)	Floodplain-corrected total yield (range)[f] (t/km²/yr)	Denudation rate (average)[g] (mm/yr)	Floodplain-corrected denudation rate (average)[h] (mm/yr)
REQ[1]	Requena	Ucayali	1	36.0	23.8	04–06	205	–	569	863	0.21	0.32
TAM[1]	Tamshiyacu	Upper Solimões	2	73.3	39.2	04–06	413	–	563	1054	0.21	0.39
BEL[2]	Bellavista	Napo	3	10.1	1.8	01–05	47	–	463	2627	0.17	0.97
MAN[3,5,6,8,16]	Manacapuru	Lower Solimões	4	227.0	50.0	82–84; 83–00; 95–98; 98–99; 02–03	403–734	106	224–370	1018–1680	0.11	0.50
PAR[4,5,6,16]	Paricatuba	Negro	5	83.2	16.2	82–84; 95–98; 98–99; 02–03	8.0–9.0	4.1	15–16	75–81	0.006	0.029
B10[7]	Confluence	Branco	6	21.3	14.7	96 and 98	3.3	–	15	22	0.01	0.01
IR[6,8,16]	Amatari	Amazon	7	315.4	62.8	74–89; 82–84	783–787	112	248–285	1424–1430	0.11	0.53
FVA[4,5,8,9,16]	Fazenda Vista Allegre	Madeira	8	133.6	28.2	74–89; 84–94; 95–98; 98–99; 02–03	151–715	19	127–550	603–2602	0.13	0.59
PVL[10,11]	Porto Velho	Madeira	9	95.4	26.0	78–93	230	–	241	883	0.09	0.33
AB[11,12]	Rurrenabaque	Upper Beni	10	6.8	6.8	69–90; 99	212–300	5.2	3190–4488	3190–4488	1.42	1.42
CE[11]	Cachuela Esperanza	Lower Beni	11	28.3	6.8	83–90	191	20	744	3093	0.28	1.15
AP[11]	Grande	Upper Mamoré	12	6.0	6.0	76–90	138	4.8	2392	2392	0.89	0.89
GM[11]	Guayaramerin	Lower Mamoré	13	59.9	12.3	83–90	66	14	138	672	0.05	0.25
VG[11]	Itenez	Guaporé (Mamoré)	14	35.4	35.4	83–90	1.7	2.7	13	13	0.005	0.005
OBI[3,6,8,13,14,16]	Óbidos	Amazon	16	508.8	94.7	79–98; 82–84; 95–98; 95–03; 95–07	556–1322	128	134–285	722–1531	0.08	0.42
IT[3,15,16]	Itaituba	Tapajós	18	59.8	23.8	97	1.4–4.3	6.3	13–18	33–44	0.006	0.014

[1]Guyot et al. (2007a).
[2]Laraque et al. (2009).
[3]Filizola and Guyot (2009).
[4]Filizola (2003).
[5]Laraque et al. (2005).
[6]Meade (1985).
[7]Moreira-Turcq et al. (2003).
[8]Dunne et al. (1998).
[9]Guyot et al. (1996; only suspended load).
[10]Guyot et al. (1999).
[11]For these stations, suspended and specific dissolved loads are from Guyot et al. (1996).
[12]Maurice-Bourgoin et al. (2002).
[13]Guyot et al. (2005).
[14]Martinez et al. (2009).
[15]Seyler and Boaventura (2003).
[16]Specific dissolved loads for these stations are from Gaillardet et al. (1997).
[a]Gauging station code as in references.
[b]ID as in Table 3. The ID enables comparing gauging and cosmogenic load data from the same location.
[c]Gauging period for dissolved loads from Guyot et al. (1996) is identical to that listed for suspended loads; the data from Gaillardet et al. (1997) were acquired during sampling cruise in May 1989.
[d]Range always gives minimum and maximum values for given reference suit; estimates on bedload are not included.
[e]Dissolved loads are surface samples.
[f]Includes suspended and dissolved yields, calculated using sediment source area only (e.g., excluding floodplain area).
[g]Average denudation rate calculated from total yield range and a density of 2.7 g/cm³ for denudation rates.
[h]Calculated from floodplain-corrected total yield range and a density of 2.7 g/cm³ for denudation rates.

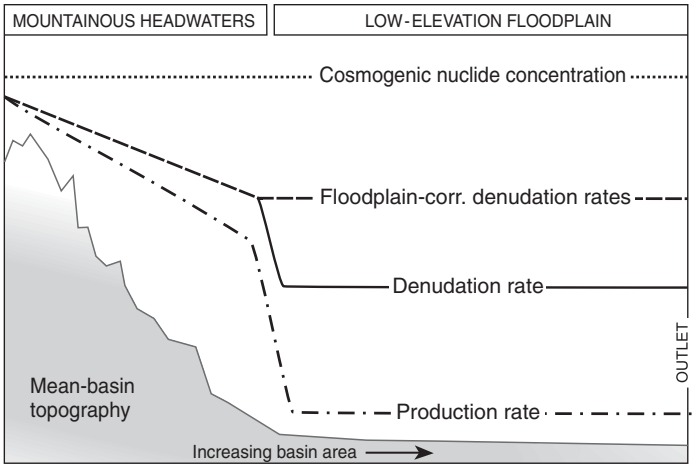

Figure 2. Schematic method for the calculation of floodplain-corrected (corr.) denudation rates in depositional basins, for the case that nuclide concentrations are uniform throughout the basin.

present study, we solemnly utilize the $^{26}Al/^{10}Be$ ratio to identify and exclude sediment fractions that have experienced such long-term burial, so that a representative hinterland denudation rate can be calculated in all cases where such indications are absent.

^{10}Be CONCENTRATION AND $^{26}Al/^{10}Be$ RATIOS RESULTS

Grain-Size Dependency as Fingerprint of the Sediment Source Areas

Figure 3 summarizes the ^{10}Be concentration data in the Amazon basin relevant for this study; respective nuclide concentrations and 1σ uncertainties (ranging usually between 4% and 9%) can be found in Table 1.

Figure 3, panels 1–3 show cosmogenic nuclide concentrations of the Peruvian Andes. Panel 4 of Figure 3 shows ^{10}Be concentrations measured in sediment sampled upstream of the Negro confluence from the Solimões River at Manacapuru. Panels 5 and 6 of Figure 3 give nuclide concentrations of the Negro and Branco rivers, respectively, which drain the Guyana Shield. Panel 7 of Figure 3 gives ^{10}Be concentrations of the Amazon River at Iracema, and Panel 8 of Figure 3 gives ^{10}Be concentrations of the Madeira River at its confluence with the Amazon River. Panels 9–13 in Figure 3 summarize the available ^{10}Be data in the Bolivian Andes (upper Madeira basin) as published by Wittmann et al. (2009). Panel 14 of Figure 3 denotes the nuclide concentrations for upper Madeira tributaries that drain the Brazilian Shield. Panels 15 and 16 of Figure 3 give again ^{10}Be concentrations of the main Amazon River at Parintins and near Óbidos, respectively, and Panel 17 of Figure 3 gives nuclide concentrations of a central Amazonian floodplain system (the "Varzea do Curuai") near Óbidos as published in Wittmann and von Blanckenburg (2009). Panels 18 and 19 of Figure 3 give ^{10}Be concentrations representative of the Brazilian Shield, e.g., of the lower Tapajós River at its confluence with the Amazon River at Santarem, and of the upper Tapajós headwater basins, respectively.

For comparison with data from central Amazonian rivers, we calculated an Andean load-weighted ^{10}Be nuclide concentration of 5.2×10^4 ats/$g_{(Qz)}$ from the data (presented in panels 1, 2, 3, 10, and 12 of Fig. 3), which include all major Andean tributaries of the Marañón, Ucayali, Napo, Beni, and Mamoré rivers and integrates over ~95% of the total Andean area that drains to the Amazon basin (see Appendix DR3 [see footnote 1] for details on load-weighting calculation). Other sediment-providing areas to central Amazonian rivers are the Guyana and Brazilian shields. In the Guyana Shield headwaters, cosmogenic ^{10}Be measurements for the Branco River yield high nuclide concentrations at an average of 39.3×10^4 ats/$g_{(Qz)}$ (n = 12; Fig. 3, Panel 6). An analysis of cosmogenic nuclide variations with grain size shows that the finer fractions mostly have higher nuclide concentrations in Branco River sediment. In the Brazilian Shield headwaters, rivers draining the upper Madeira basin (Panel 14, Fig. 3) give a load-weighted average ^{10}Be concentration of 18.7×10^4 ats/$g_{(Qz)}$ (n = 4), and rivers that drain the upper Tapajós basin (Panel 19, Fig. 3) give a load-weighted average ^{10}Be concentration of 15.4×10^4 ats/$g_{(Qz)}$ (n = 10). These average nuclide concentrations are significantly lower than those of the headwaters of the Guyana Shield. For this region, no trend in nuclide concentrations with grain size is observed.

The major findings concerning nuclide concentrations as a function of grain size are as follows. (1) Measured ^{10}Be concentrations of the Solimões River at Manacapuru (Fig. 3, Panel 4) show very little dependency on grain size, with an average ^{10}Be concentration of eight samples of 6.7×10^4 ats/$g_{(Qz)}$. (2) At sampling locations on the Amazon River downstream of the Negro confluence (e.g., Iracema and Parintins, Fig. 3, Panels 7 and 15), we observe a significant increase in the variability of ^{10}Be concentration with grain size. The finest analyzed fractions (mostly 125–250 µm, sometimes also 250–500 µm) always yield significantly lower ^{10}Be nuclide concentrations than the 500–800 µm fraction. At Parintins, for example, an average ^{10}Be concentration of 7.3×10^4 ats/$g_{(Qz)}$ (n = 4) was measured in finer fractions (125–500 µm), whereas one sample for the coarsest analyzed 500–800 µm fraction yields a nuclide concentration of 16.7×10^4 ats/$g_{(Qz)}$ (see Table 1). (3) This trend is also observed in the lower Madeira River (draining the Bolivian Andes as well as the Brazilian Shield) close to its confluence with the Amazon River (Panel 8 in Fig. 3). An average nuclide concentration for the 125–250 µm fraction is 5.6×10^4 ats/$g_{(Qz)}$ (n = 2), the 250–500 µm fraction is 9.0×10^4 ats/$g_{(Qz)}$ (n = 3), and one sample for the 500–800 µm fraction is 21.8×10^4 ats/$g_{(Qz)}$. (4) Some rivers in central Amazonia display a different behavior. In the case of the lower Negro near the Amazon confluence (Fig. 3, Panel 5), finer grain-size fractions yield higher nuclide concentrations, similar to the pattern observed in Negro River headwaters drained by the Branco River. The Negro draining the Guyana Shield thus shows an opposite trend than rivers that drain Andean territory. Moreover, ^{10}Be concentrations of the lower Negro are 7.8×10^4 ats/$g_{(Qz)}$ (n = 6). These concentrations are ~5 times lower than those of the Branco River in the Guyana Shield headwaters. (5) In the Tapajós near the Amazon confluence (Fig. 3, Panel 18), nuclide concentrations do not vary with grain size. Measured ^{10}Be nuclide concentrations for the lower Tapajós are significantly lower than the Tapajós headwaters in the Brazilian Shield. Near the Amazon confluence, the lower Tapajós shows a mean nuclide concentration of 9.7×10^4 ats/$g_{(Qz)}$ (n = 3).

Identification of Sediment Burial from $^{26}Al/^{10}Be$ Ratios

Aside from cosmogenic ^{10}Be, we measured cosmogenic ^{26}Al nuclide concentrations in selected samples to identify burial of sediment

from the $^{26}Al/^{10}Be$ ratio (see Table 1 and "Methods"). Burial results in differential decay of isotope pairs due to differences in half-lives (Granger and Muzikar, 2001; Granger, 2006). The surface production ratio of $^{26}Al/^{10}Be$ ranges between 6.5 and 7.2 (the exact value is currently debated; see Goethals et al., 2009). Samples yielding $^{26}Al/^{10}Be$ ratios below these values have experienced burial at some stage in their sedimentary history. For detrital fluvial sediment, repeated burial and relocation are possible, and thus the measured $^{26}Al/^{10}Be$ ratio integrates over different burial events. Our $^{26}Al/^{10}Be$ ratios therefore yield minimum estimates of burial depth and duration (Balco et al., 2005; Granger, 2006; Wittmann and von Blanckenburg, 2009). All samples that show $^{26}Al/^{10}Be$ ratios <6.5 were excluded from the calculation of basin-wide denudation rates, even in cases of slight burial, because these samples do not represent the modern erosion signal. In Table 1 (last column), we state explicitly which samples allowed in our view the calculation of denudation rates.

For the Amazon mainstream along the 800 km transect from Manacapuru to Óbidos, burial ratios are in general somewhat lower than the surface ratio of ~6.5. At Manacapuru (Man) for example, a mean $^{26}Al/^{10}Be$ ratio of 5.3 ± 1.0 was measured for three samples that were analyzed for ^{26}Al. Only sample Man 0.2a does not display burial (although within a high uncertainty caused by high natural Al contents of ~1.5 mg; see Table DR1 [footnote 1]). For samples at Parintins (Par), the two samples analyzed for ^{26}Al show slight burial (average $^{26}Al/^{10}Be$ ratio of 6.2 ± 1.9).

In the Guyana Shield (Branco River), $^{26}Al/^{10}Be$ ratios of 5.4 ± 0.5 (n = 5) indicate that at least 20% of the stream sediment is derived from buried sources, when mixing calculations between nonburied and buried end member sources are applied. For this data set, only sample Br 1a shows minimal burial ($^{26}Al/^{10}Be = 6.2 \pm 0.5$; see Table 1). Other Branco samples were buried for durations of >0.5 to 2 m.y. and depths of 3–5 m, so that the corresponding basin-wide denudation rate of 0.012 mm/yr is a minimum estimate of the prevailing denudation rate from

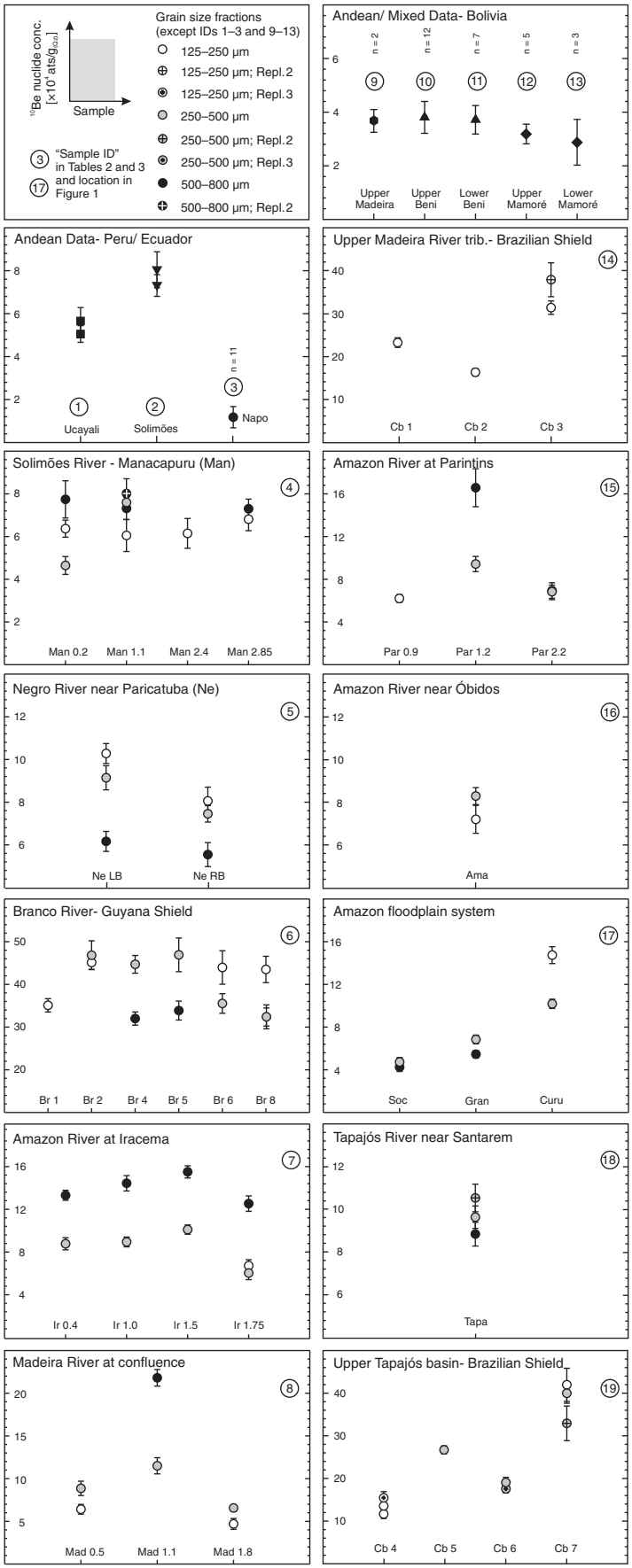

Figure 3. In situ–produced cosmogenic ^{10}Be nuclide concentrations (in × 10^4 ats/$g_{(Qz)}$) of samples relevant for this study. Circled numbers correspond to locations shown in Figure 1. Data from panels 9–13 are taken from Wittmann et al. (2009), and data from panel 17 are taken from Wittmann and von Blanckenburg (2009). See text for more explanation.

sample Br 1a. Initial nuclide concentrations (that were representative of a steady-state erosion rate prior to burial) will have significantly changed due to long-term deep burial in these intensely weathered areas, so that the measured nuclide concentration almost certainly underestimates steady-state nuclide concentrations.

In the Varzea do Curuai floodplain setting in central Amazonia, Wittmann and von Blanckenburg (2009) used $^{26}Al/^{10}Be$ ratios to distinguish between Miocene floodplain (sample Curu) that has not been reworked by the Amazon River recently, and the modern Amazon floodplain (samples Gran and Soc; see Table 1 for their ^{10}Be and Table DR1 [footnote 1] for their ^{26}Al nuclide concentrations), which evidently receives sediment from the main Amazon River. These results indicate that burial of more than 5 m.y. in Miocene floodplain systems occurs (see Wittmann and von Blanckenburg, their fig. 4C). We included the data from samples Gran and Soc into our denudation rate/sediment load calculations (see Table 3), because these samples reflect the active part of the floodplain that receives fine-grained, mostly unshielded sediment from the Amazon, whereas sample Curu has experienced significant burial prior to erosion.

SEDIMENT PROVENANCE AND MIXING IN THE AMAZON BASIN

The preceding presentation of our new data has shown that (1) in some samples strong grain-size dependencies of ^{10}Be concentrations exist, and (2) some samples display a significant $^{26}Al/^{10}Be$ signature of burial. These patterns are mostly reproducible phenomena that we synthesize here.

Assessment of Source Area Grain-Size Dependency

Upstream of the confluence between the Negro and the Solimões (represented by samples Man at Manacapuru), no dependence in the ^{10}Be concentration with grain size can be detected. Below the confluence at Iracema, ^{10}Be concentrations depend on grain size, and this pattern is preserved from thereon downstream. Where Andean sediment is incorporated (Madeira, Amazon at Iracema, Parintins, and Óbidos), the coarse grain sizes contain higher nuclide concentrations than the fine grains. In all settings that drain shield areas or Neogene lowland formations but that lack the Andean hinterland (Xingu, Branco, and Negro), the finer grains contain higher nuclide concentrations than the coarser sediment.

In cases of the lower Negro and Tapajós rivers (sampled close to the Amazon confluence), the exceptionally low nuclide concentrations (when compared to their headwater concentrations) might be due to very strong Amazon discharge events that regularly block water and sediment delivery from the Negro and Tapajós rivers; thus, these low nuclide concentrations are diluted from main Amazon River sediment input. Concerning grain size, the Negro shows downstream fining, which is due to the successive filling of basins in upper reaches with coarser sediment that does not reach the Negro downstream section (Latrubesse and Franzinelli, 2005). Sediment provenance and grain-size analysis for the lower Negro near the Amazon confluence (Franzinelli and Igreja, 2002; Latrubesse and Franzinelli, 2005) shows that especially coarser sand does not originate from Guyana Shield areas, but from Cretaceous continental deposits of the Alter do Chão Formation, which mainly consists of quartz-rich red clayed sandstones, siltstones, and claystones (Latrubesse and Franzinelli, 2005).

Aside from the special cases of the lower Negro and Tapajós, we interpret the observed grain-size–specific ^{10}Be concentrations in terms of provenance. In the non-Andean catchments, coarse quartz grains are the main survivors of slow (>100 k.y.) weathering of the cratonic shields (Dosseto et al., 2006a). Where Andean sediment is present, we are dealing with a binary mixture where coarse grains are being supplied by the cratonic and non-Andean landscapes, while fine grains with low nuclide concentrations survive sediment transport and comminution along the long route from the Andes to the central Amazon basin. This observation is supported by grain-size analysis of these different regimes by Franzinelli and Potter (1983) and Potter (1994).

Signatures of Sediment Burial from $^{26}Al/^{10}Be$ Ratios

All cratonic and Andes-draining rivers carry formerly buried sediment. In cratonic headwater areas and in the lower Guyana Shield, we generally observe the strongest burial signals with $^{26}Al/^{10}Be$ ratios well below 6.5. In the Guyana Shield, rivers are in general sediment depleted. Therefore, any contribution of deeply buried sediment would dilute the source area signal, resulting in the observed very low $^{26}Al/^{10}Be$ nuclide ratios. Low $^{26}Al/^{10}Be$ ratios are however also observed in the Amazonian lowlands, where all sampled rivers carry buried sediment at variable fractions. Lowest $^{26}Al/^{10}Be$ ratios and therefore longest burial durations are observed in Miocene sediment of isolated floodplain deposits (present in the "Varzea do Curuai"). The presence of formerly buried sediment in active central Amazonian streams could therefore be explained by the admixture of very old, buried sediment of at least Tertiary age from non-Andean tributaries (e.g., the cratons), or, alternatively, from incorporation of sediment that was remobilized recently from large depths of very old (i.e., late Miocene), formerly isolated floodplain deposits. This assessment shows that an analysis of ^{26}Al along with ^{10}Be could improve our understanding of sediment transport in larger basins; moreover, we suggest that these analyses should be routinely carried out when using in situ–produced ^{10}Be for denudation rate deduction in large river basins.

ANDEAN DENUDATION RATES AS PRESERVED IN ^{10}Be NUCLIDE CONCENTRATIONS FROM FINE-GRAINED CENTRAL AMAZONIAN SEDIMENT

A load-weighted average ^{10}Be concentration for central Amazonian rivers (IDs 4, 7, 8, 15, 16, and 17) is $6.2 \pm 0.5 \times 10^4$ ats/$g_{(Qz)}$ (1σ, n = 16). We calculated this concentration from all fine grain-size fractions <500 µm and from samples that did not contain a burial signal (see Table 3 for details on sample exclusions). We can now compare this ^{10}Be concentration to that of the major Andean tributaries, which is $5.2 \pm 0.5 \times 10^4$ ats/$g_{(Qz)}$ (1σ). The difference between Andean and central Amazonian nuclide concentrations could be attributed to input of fine-grained sediment from other rivers (e.g., Purus and Juruá rivers) for which ^{10}Be nuclide concentrations have not been measured. Nevertheless, we observe that the ^{10}Be concentration of the finest analyzed fraction is relatively steady along the entire course of the trunk stream (Fig. 4A). Given that this Andean nuclide concentration appears to be preserved over the length of the entire Amazon stream, one may calculate floodplain-corrected denudation rates, using only the Andean area for production rate derivation (cf. Wittmann et al., 2009, and Appendix DR4 [see footnote 1]). The average ^{10}Be nuclide concentration of all Andean tributaries of the upper Solimões, Ucayali, Napo, Beni, and Mamoré rivers (see Table 3) translates to a flux-weighted mean denudation rate of 0.37 ± 0.06 mm/yr. This average value compares to 0.24 ± 0.02 mm/yr (Fig. 4B) for central Amazonian river samples, excluding formerly buried and coarse sediment, and also disregarding floodplain and cratonic shield terrain for production rate calculation. We conclude that ^{10}Be-derived denudation rates from fine-grained sediment in the Amazon trunk stream approach Andean denudation rates. This finding is summarized in Figure 5, where for all major tributaries, average floodplain-corrected denudation rates are presented.

TABLE 3. AVERAGED COSMOGENIC NUCLIDE AND PRESENT-DAY SEDIMENT LOAD DATA USED FOR SEDIMENT BUDGET CALCULATION

			Cosmogenic nuclide-derived data used for calculation of loads Q_{CN} (this study) (see Table 1)					Published modern sediment loads Q_M (see Table 2)	
ID	River or setting	Gauging station code	Number of analyses included in denudation calculation[a]	$N_{included}$ of / N_{total}[a]	Average cosmogenic nuclide concentration[b] ($\times 10^4$ at/g$_{(Qz)}$)	Sediment source area[c] ($\times 10^4$ km^2)	Floodplain-corrected cosmogenic denudation rate[d] (mm/yr)	Apparent cosmogenic load[e] (Mt/yr)	Average sediment load[f] (Mt/yr)	Floodplain-corrected denudation rate[g] (mm/yr)
1	Ucayali at Requena	REQ	2	1.0	5.3 ± 0.4	19.8	0.34 ± 0.04	181	205	0.32
2	Upper Solimões at Tamshiyacu	TAM	2	1.0	7.7 ± 0.5	39.2	0.20 ± 0.02	216	413	0.39
3	Lower Napo near Iquitos	BEL	11[h]	1.0	1.2 ± 0.2	1.8	0.87 ± 0.38	42	47	0.97
4	Lower Solimões at Manacapuru	MAN	3	0.3	6.4 ± 0.4	50.0	0.24 ± 0.02	326	675	0.50
5	Negro near Paricatuba	PAR	Minim. E, n = 6	0.0	7.8 ± 1.8	16.2	0.040 ± 0.003	17	13	0.029
6	Branco, Guyana Shield (Upper Negro basin)	B10	Minim. E, n = 1	0.1	35.1 –	14.7	0.014 ± 0.001	5.5	3.3	0.008
7	Amazon at Iracema	IR	2	0.2	6.4 ± 0.5	62.8	0.24 ± 0.03	412	897	0.53
8	Lower Madeira at confluence	FVA	3	0.5	5.9 ± 1.0	28.2	0.21 ± 0.02	157	452	0.59
9	Upper Madeira at Porto Velho	PVL	3[i]	1.0	3.7 ± 0.4	28.2	0.28 ± 0.04	213	230	0.33
10	Upper Beni at Rurrenabaque	AB	2[j]	1.0	3.8 ± 0.2	6.8	0.38 ± 0.07	70	261	1.42
11	Lower Beni at Cachuela Esperanza	CE	12[k]	1.0	3.7 ± 1.6	6.8	0.45 ± 0.07	82	210	1.15
12	Upper Mamoré basin (Grande River)	AP	7[l]	1.0	3.2 ± 4.8	7.9	0.56 ± 0.09	119	143	0.89
13	Lower Mamoré at Guayaramerin	GM	5[m]	1.0	2.9 ± 2.0	12.3	0.55 ± 0.19	182	83	0.25
14	Upper Madeira River tributary, Brazilian Shield	VG	2	0.5	19.7 ± 5.0	28.2	0.024 ± 0.002	18	4.4	0.005
15	Amazon at Parintins	–	3	0.6	6.6 ± 0.6	94.7	0.21 ± 0.02	540	–	–
16	Amazon near Óbidos	OBI	1	0.5	7.2 –	94.7	0.20 ± 0.02	505	1067	0.42
17	Amazon floodplain system	–	5[n]	0.7	5.2 ± 1.0	94.7	0.28 ± 0.03	725	–	–
18	Tapajós near Santarém	IT	2	0.7	10.1 ± 0.6	23.8	0.040 ± 0.003	26	9.1	0.014
19	Upper Tapajós basin, Brazilian Shield	–	6	0.6	15.9 ± 2.8	23.8	0.028 ± 0.004	18	–	–

[a]In some cases, the number of analyses deviates from total number measured, because some central Amazonian samples were excluded for denudation rate calculation due to burial (see Table 1 last column); "minim. E" denotes samples that give minimum denudation rates, because all these samples were affected by burial [these are: all Negro (ID 5) and all but Br 1a (ID 6)].

[b]Gives average nuclide concentration (with standard deviation) used to calculate average cosmogenic nuclide-derived denudation rate.

[c]Denotes Andean area >200 m elevation, used to calculate floodplain-corrected denudation rates.

[d]Average floodplain-corrected denudation rate with 1σ uncertainty. For Amazonian lowland rivers, rates were calculated excluding coarse grain sizes and samples that display burial (see footnotes and Table 1 last column).

[e]Calculated from averaged floodplain-corrected denudation rates and a density of 2.7 g/cm^3.

[f]Average load calculated from suspended load minimum and maximum values plus dissolved loads given in Table 2.

[g]Calculated from average total loads using a density of 2.7 g/cm^3 and the sediment source area.

[h]Average of Napo floodplain samples (see Wittmann, 2008); data included in Andean weighted average denudation calculation (see Appendix DR2 [see footnote 1]).

[i]Average from Upper Madeira samples (Mad 19a, 20a-1, and 20a-2; see Wittmann et al., 2009).

[j]Average from Upper Beni samples at Rurrenabaque (Be 1a and 1b; see Wittmann et al., 2009); data included in Andean weighted average denudation calculation (see Appendix DR2 [see footnote 1]).

[k]Average from Lower Beni samples (Be 2 to 17; see Wittmann et al., 2009).

[l]Load-weighted avg. from Upper Mamoré (GR 19, GR 25, PIR 18, CHA 23, ICH 21, and MAN 15; see Wittmann et al., 2009); included in Andean weighted average calculation (see Appendix DR2 [see footnote 1]).

[m]Load-weighted average from Lower Mamoré samples (GR 17, MAR 16 and 18; see Wittmann et al., 2009).

[n]Representative for Amazon flowing through Curuai floodplain. Coarse grain sizes stem from within the floodplain, thus all Soc and Gran samples (but not Curu) were included in average denudation rate calculation.

SEDIMENT BUDGET FOR THE AMAZON BASIN

In Table 3 and Figures 5 and 6, we summarize our cosmogenic nuclide-derived sediment budget for all major tributaries. The burial-free average denudation rate from fine grain sizes (~0.24 mm/yr, see "Andean denudation rates as preserved in ^{10}Be nuclide concentrations from fine-grained central Amazonian sediments") calculated from central Amazonian nuclide concentrations and an Andean area of 94.7×10^4 km^2 translates to an average cosmogenic nuclide-derived sediment load (Q_{CN}) of 610 Mt/yr. If none of this sediment were lost by net storage into the floodplain, this value would represent the average annual sediment load passing Óbidos. The basin of the Solimões at Manacapuru contributes a Q_{CN} of ~330 Mt/yr, the Madeira basin near the Amazon confluence contributes a Q_{CN} of 160 Mt/yr, and the lower Negro and Tapajós draining cratonic areas together contribute a minimum Q_{CN} of ~45 Mt/yr (see Fig. 6). The budget shows that the sums of the individual reaches are consistent with respect to the total flux at Óbidos, except for a small difference that is due to the minor sediment discharge of lowland rivers such as the Purus and Juruá rivers and the Andean-draining Putumayo-Iça River that have not been sampled for cosmogenic nuclide analysis. This assessment using cosmogenic nuclides shows that our mass budget is internally consistent, and it demonstrates that the sediment debouched from the Andes is indeed the dominant sediment source for the central Amazon region as suggested by Gibbs (1967), Meade (1985), and Meade et al. (1985) with additions from non-Andean cratonic source areas being minor.

COMPARISON BETWEEN COSMOGENIC NUCLIDE-DERIVED AND MODERN SEDIMENT LOADS

When compared with short-term modern loads calculated from suspended and dissolved sediment (Q_M), most of our apparent loads Q_{CN} agree relatively well (within a factor of ~2, Table 3 and Fig. 7). This trend is especially observed for central Amazonian (lowland) rivers, where a divergence by a factor of 2 results only from calculating an average value (1067 Mt/yr suspended and dissolved load at Óbidos, Table 3) from the range given in Table 2. This range is largest at the outlet of the Amazon basin (at Óbidos; lowest published value 556 Mt/yr compared to the highest published value of 1322 Mt/yr), and thus already incorporates an internal variance in gauging-derived fluxes of more than ±50%. Taking a "longer"-

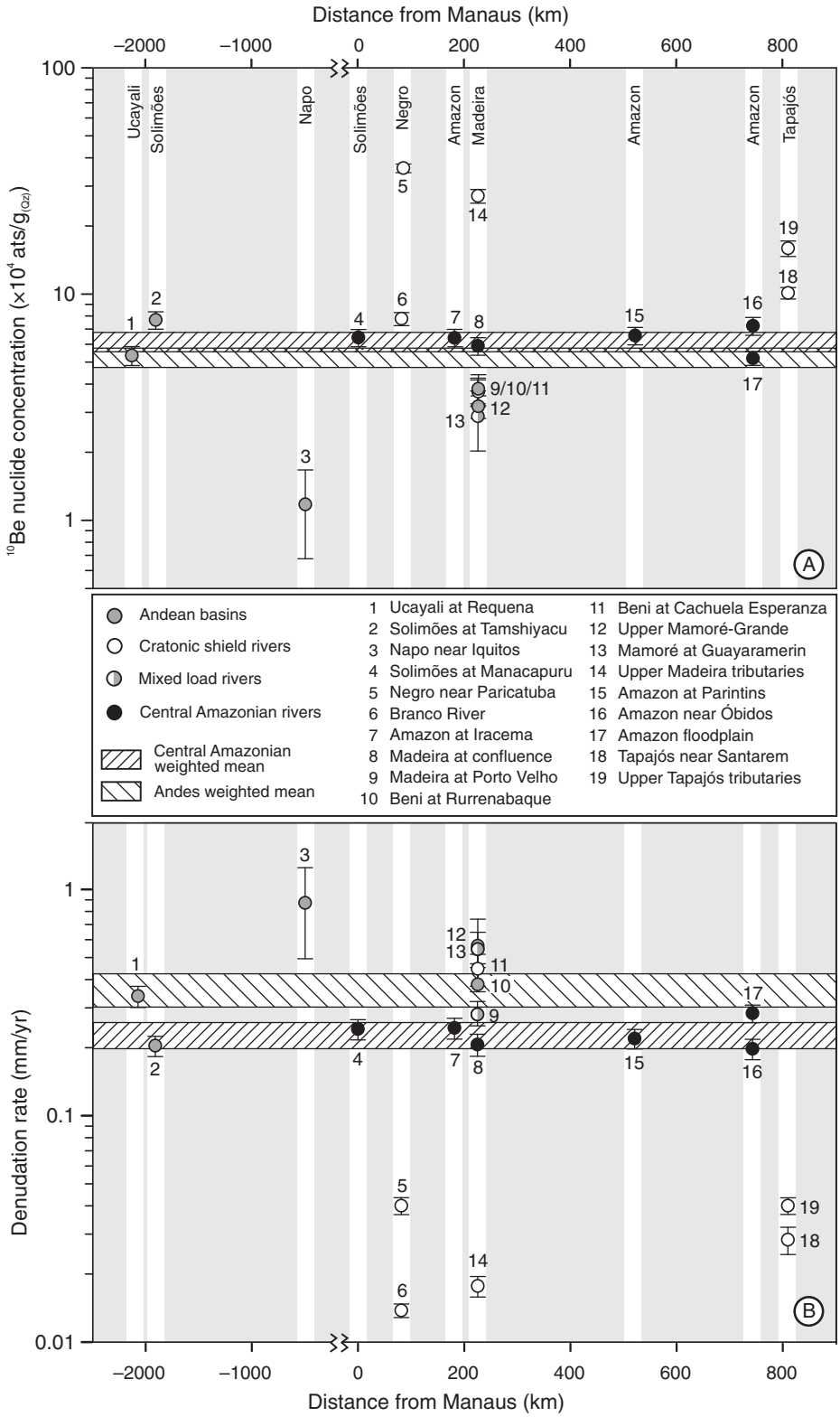

Figure 4. (A) Summary of ^{10}Be nuclide concentrations (× 10^4 ats/g$_{(Qz)}$) of fine-grained samples unaffected by burial versus distance from Manaus (in km). (B) Respective denudation rates (mm/yr) that are corrected for floodplain area where necessary (see Fig. 2 and Appendix DR4 [footnote 1] for more details on floodplain-correction). In both plots, the Andean load-weighted mean (calculated from IDs 1, 2, 3, 10, and 12) and the central Amazonian load-weighted mean (calculated from IDs 4, 7, 8, 15, 16, and 17) are given.

term modern load estimate (i.e., 556 Mt/yr averaged over a maximum integration time of 19 yr; see Filizola and Guyot [2009] and Table 2), a 100% agreement between Q_M and Q_{CN} would be achieved. The agreement within a factor of ~2 thus can be seen as an upper limit, and it shows that the central Amazon basin may not be one in which sediment is deposited on kyr time scales, or the system may be switching to be more erosive recently. This finding is in agreement with Maurice-Bourgoin et al. (2007), who concluded that the central Amazonian floodplain system is not an efficient sediment trap.

In systems that are dominated by Andean sediment discharge, especially in the Bolivian Andes (Beni system), modern loads are higher than cosmogenic nuclide-derived fluxes by a factor of ~4. If different integration time scales for both methods are the main source of this variance (see discussion below and in "The long-term stability of output fluxes as caused by diffusive-like floodplain buffering"), it is necessary to note that the modern load record of the upper Beni system (e.g., at Rurrenabaque, see Table 2) presents one of the longest gauging records in the Amazon basin (1969–1990). In the Peruvian Andes (e.g., at Tamshiyacu), where Q_M is higher than Q_{CN} by a factor of ~2, suspended sediment gauging has been carried out for the period 2004–2006 only (see Table 2).

In sediment-starved systems like the Tapajós and Guaporé rivers, the agreement between modern loads Q_M and cosmogenic-derived Q_{CN} is somewhat weaker. In these systems, Q_{CN} are generally higher than Q_M with an average deviation factor of ~3. In the Branco and Negro rivers, the agreement is better, although our cosmogenic nuclide-derived loads give minimum estimates only for these rivers.

We conclude that the agreement between modern sediment fluxes Q_M and long-term fluxes Q_{CN} is much poorer in the sediment source areas than in central Amazonia. Therefore, the similarity in exported Q_M and Q_{CN} fluxes at the Amazon outlet cannot stem from similar erosion rates already present in the sediment source areas.

Bridging Time Scales: From Short-Term Modern over Cosmogenic Nuclides to Long-Term Fission-Track Denudation Estimates

These observations can be interpreted in relation to the differences in time scale of both methods. We assign a maximum integration time scale of ~14 k.y. (Dosseto et al., 2006b) to Andean-derived, ^{10}Be-based sediment loads Q_{CN} of the central Amazon basin, because this is the maximum transfer time of suspended particles

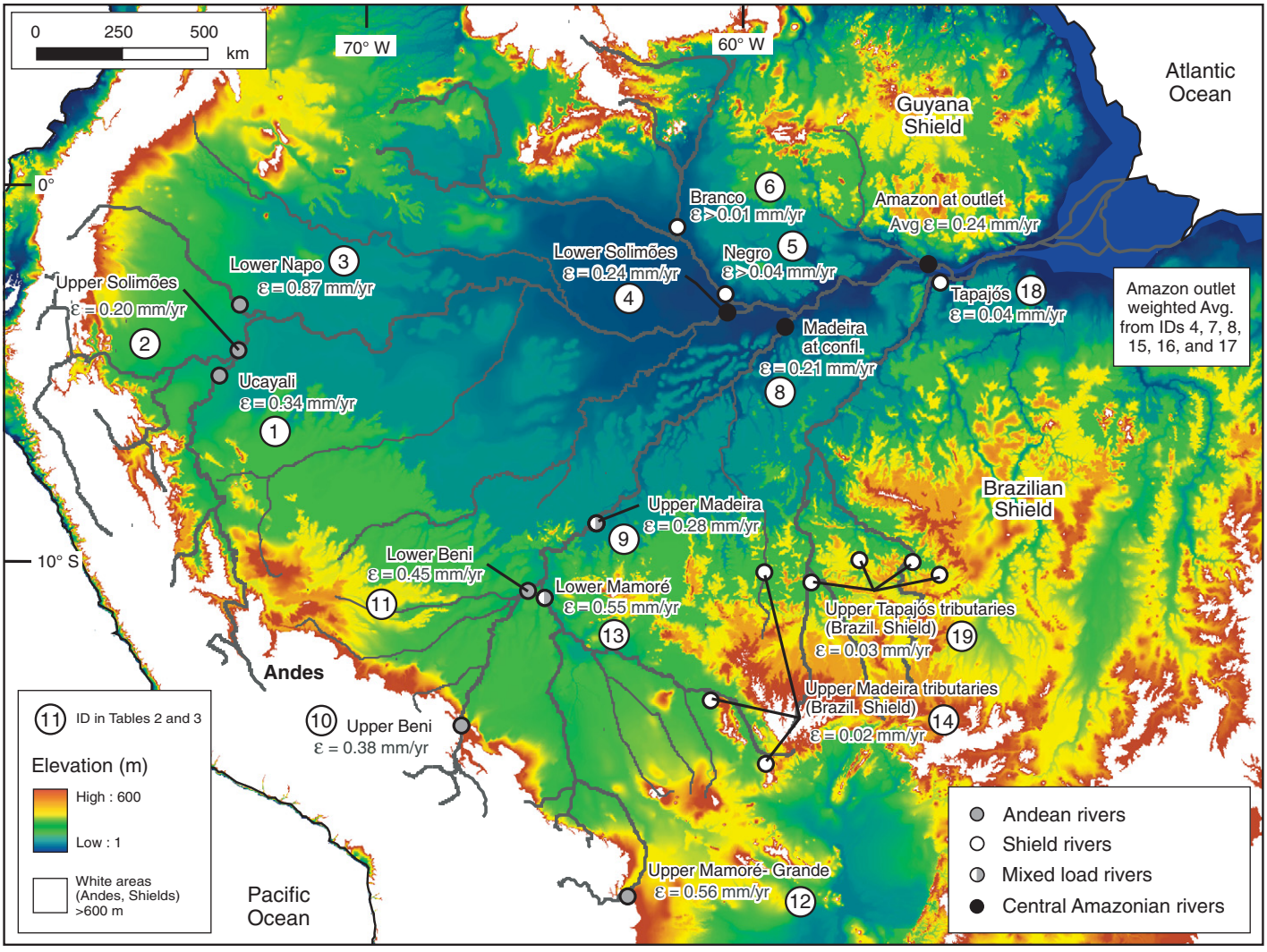

Figure 5. Average denudation rates (ε, in mm/yr) from ^{10}Be nuclide concentrations for major tributaries of the Amazon basin. The value calculated for the Amazon outlet near Óbidos denotes a weighted average from IDs 4, 7, 8, 15, 16, and 17, which does not include coarser grain sizes and burial-affected samples (see text for explanation).

from the Bolivian Andes to the central Amazon plain carried by the Madeira River. In the shields and in very old floodplain systems that are usually isolated from the modern river, this assigned time scale may be an underestimation (Mathieu et al., 1995; Dosseto et al., 2006a). A time scale for the erosion of sediment particles in the Andean source area is given by the cosmogenic "apparent age" (Table 1; von Blanckenburg, 2005) which is ~1.6 k.y. for an average Andean denudation rate of 0.37 mm/yr. This average Andean denudation rate is similar to long-term (up to 20 m.y.) denudation estimates from apatite fission-track (AFT) analysis: a denudation rate of 0.3 mm/yr has been measured by Safran et al. (2006) in the high Bolivian Andes (Eastern Cordillera and Subandes); a range of 0.2 to 0.7 mm/yr (with a highly disputed increase to 0.7 mm/yr at 10–15 m.y.) has been suggested by Benjamin et al. (1987) for the same area. Barnes et al. (2008) have recently measured AFT-based exhumation rates of ~0.1–0.6 mm/yr in the more southern Bolivian Andes and Subandes. This agreement between long-term rates from fission-track and shorter, kyr-scale cosmogenic nuclide-based rates hints at cosmogenic nuclides being able to capture the long-term features of a mountain belt (Wittmann et al., 2009). Sediment gauging-derived fluxes on the other hand integrate only over the gauging period and cannot be extrapolated to longer time scales (Walling and Webb, 1981; Walling, 1983). It is known from statistical analysis of environmental time series data that a certain time interval in sampling is required to recognize the magnitude and recurrence interval of natural variations. Assume, for example, that high-magnitude, low-frequency sediment discharge events take place at a regular recurrence interval. Then the period of gauging necessary to capture the full amplitude of an interval is required to be at least half of the recurrence interval ("Nyquist frequency," e.g., Borradaile, 2003; Jerolmack and Sadler, 2007). This minimum sampling frequency for representative sampling is dependent on the basin size and thus must be determined individually for each basin (Coynel et al., 2004). In summary, short gauging periods and low sampling frequencies (e.g., yearly) could result in sediment fluxes that in some cases could overestimate or in other cases could underestimate the real fluxes, depending on the setting, basin size, and gauging methodology used. In the following, we discuss consequences with respect

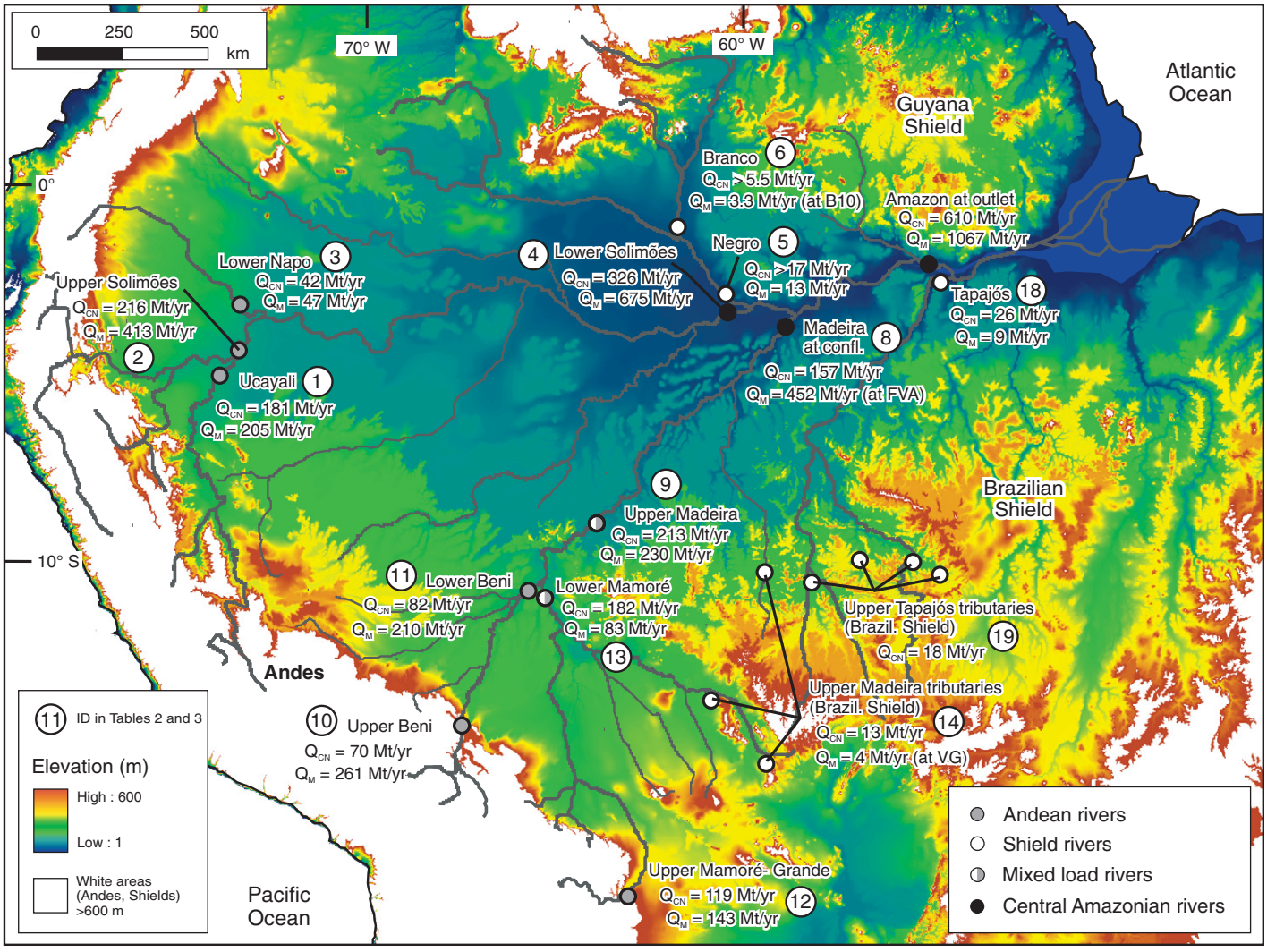

Figure 6. Sediment budget for the Amazon basin. Q_{CN} denotes sediment fluxes calculated from cosmogenic nuclides (this study), and Q_M denotes modern gauging-based fluxes from suspended and dissolved loads compiled from several different sources (see Table 2). The Q_{CN} value calculated for the Amazon outlet near Óbidos was calculated from a weighted average from IDs 4, 7, 8, 15, 16, and 17, and the Q_M value at Óbidos gives an average total load calculated from the minimum and the maximum published values at this location.

to changes in climate and sea level that arise from the different integration time scales of cosmogenic nuclide and gauging methods.

Changes in Climate Affecting Sediment Loads

Both modern and cosmogenic nuclide-derived sediment fluxes in the Andean sediment source area could be affected by changes in climate that occur within the different integration time scales of the two methods. A drier climate in the Andean source areas persisting over most of the Holocene including the Last Glacial and a wetter modern climate for the past few thousand years (Cross et al., 2000; van der Hammen and Hooghiemstra, 2000; Abbott et al., 2003) might also explain lower long-term sediment output fluxes compared to higher modern fluxes. However, the overall effect of precipitation on erosion is also a function of vegetation density, which stabilizes erosion at a certain threshold. Thus, erosion does not necessarily increase with increasing precipitation (Langbein and Schumm, 1958).

Changes in Sea Level

Changes in sea level occurring during the integration time scales could also affect sediment fluxes. During the Last Glacial Maximum (~20 k.y. ago), sea level was ~120 m below the present level, which caused deep incision of the Amazon river bed and led to an excavation of sediment deposited during earlier sea-level high stands (Mertes and Dunne, 2007; Irion et al., 2009). Approximately 11 k.y. ago, sea-level rise began to affect the Amazon basin (Irion et al., 2006), and ~3 k.y. ago, the water surface of the Amazon River attained its current elevation (Mertes and Dunne, 2007). Characteristic of high water stand periods is a reduced sediment delivery with increased rates of sedimentation, especially in the estuary of the lower Amazon River (Mertes and Dunne, 2007). The resulting variations in the Amazon floodplain configuration could potentially cause the observed divergence between Q_M and Q_{CN} (we will discuss this possibility in "The long-term stability of output fluxes as caused by diffusive-like floodplain buffering). For cosmogenic nuclide-derived loads Q_{CN}, we expect no effect by sea-level–induced changes of the floodplain, because nuclide concentrations are

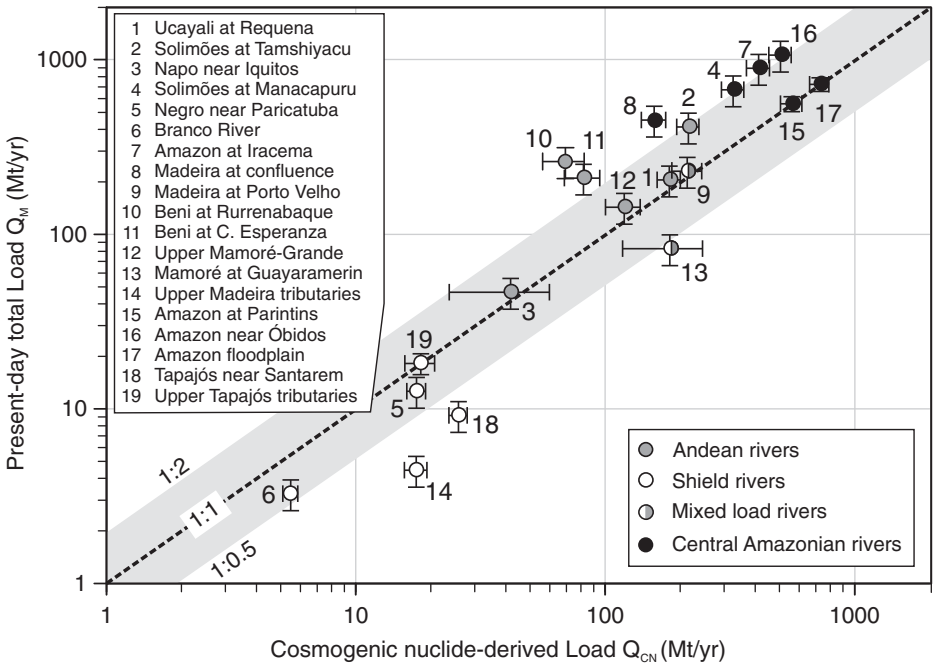

Figure 7. Comparison between cosmogenic nuclide-derived sediment load Q_{CN} (with 1σ uncertainty) and modern loads Q_M from suspended and dissolved yields (for which we assigned constant 20% uncertainty) for all major streams as well as headwater tributaries as summarized in Table 3. Andes-draining rivers are indicated by gray circles; shield-draining rivers are given by white circles, and central Amazonian rivers are shown in black. Half-filled circles indicate mixed load rivers (Mamoré at Guayaramerin and Madeira at Porto Velho, which both integrate over Brazilian Shield as well as Andean area). The dashed line indicates agreement between Q_{CN} and Q_M, and bounding lines show Q_M/Q_{CN} ratios of 2 and 0.5, respectively. Basins 15, 17, and 19 were plotted on 1:1 line, although for these basins Q_M is not available.

uniform throughout the basin from the Andes to the floodplain's outlet, thereby integrating over all floodplain changes since the Last Glacial Maximum. Modern sediment loads on the other hand may be much more sensitive to local erosion deposition disequilibria in the floodplain as the slope of the river bed is adjusted to changes in the reference water level.

It is important to discuss the potential causes for the difference in exported fluxes for these two methods; however, we would like to point out here that an agreement within a maximum factor of 2 is a relatively good agreement, given the above discussed differences. Therefore, it is interesting to note that estimations from both methods are roughly consistent with sediment discharge estimates from ^{210}Pb activity profiles in the Amazon delta on the continental shelf. For this area and with an integration time of ~1 k.y., an average flux of 630 ± 200 Mt/yr has been measured (Kuehl et al., 1986), which is within the (probably more realistic) range of 550 to 1030 Mt/yr that was later proposed by Nittrouer and Kuehl (1995).

THE LONG-TERM STABILITY OF OUTPUT FLUXES AS CAUSED BY DIFFUSIVE-LIKE FLOODPLAIN BUFFERING

We attribute the agreement of modern and long-term output fluxes for the central Amazonian system to the buffering capacity of the large Amazon floodplain. The buffering capacity of a floodplain results from negative as well as positive feedbacks between deposited alluvium and the sediment yield export from a basin. High sediment delivery to channels will either result in increasing storage of sediment, or in increasing transport of sediment. Further, increased alluvial storage results in decreased sediment export. If the sediment delivery to the river channel is, however, limited by slow upland erosion, sediment transport capacity exceeds sediment production, and thus all supplied material will be routed rapidly through the channel (Stallard, 1995). Diffusive-like buffering implies that sediment storage may result in output fluxes that are relatively unresponsive to environmental change. Intrinsic in this assumption is a persistent, accommodation-dominated regime of a large sedimentary system (Jerolmack and Sadler, 2007). If the amount of sediment stored in a floodplain is large relative to the output sediment yield, large pulses in sediment production from hinterland erosion may be buffered. Further, when hinterland sediment delivery is reduced, the stream may maintain certain sediment loads due to transportable debris stored in the floodplain (Phillips, 2003). Consequently, relative variations in sediment fluxes are minimized if the amount of alluvial storage is high relative to the rivers' transport capacity (Métivier and Gaudemer, 1999; Phillips and Slattery, 2006). In this respect our data allow for the first-order implication that large floodplains may effectively buffer against changes in erosion, whether these changes are climate or tectonic induced. The original perturbation (the hinterland erosion rate) having a large amplitude but a short period is smoothed by the time the erosion signal has passed through a large floodplain (Métivier, 1999).

The efficiency of buffering relies on the floodplain reaction time that scales with floodplain size (Métivier, 1999; Métivier and Gaudemer, 1999). We can calculate a maximum reaction time of roughly 7×10^5 yr for the Amazon floodplain that is close to the main channel following Métivier and Gaudemer (1999), by using their Equation 3 and a floodplain length of 3500 km, a floodplain width of 40 km, a maximum relief of the floodplain of 150 m, and a long-term mass flux of 300×10^6 m^3/yr, which we calculated from our cosmogenic nuclide-based average sediment load of 610 Mt/yr and a mean wet sediment density of 2.0 g/cm^3. As a consequence of this long reaction time, short-term, high-amplitude fluctuations (changes in sea level, climatic variability in source areas, and anthropogenic soil erosion in the hinterland) are smoothed by the time the denudation signal reaches the outlet of the basin.

SUMMARY

We present a sediment budget for the Amazon basin that we calculated from cosmogenic nuclide-derived denudation rates. From ~50 ^{10}Be analysis of bedload and bank sediment samples, we found that an average nuclide concentration for central Amazonian rivers is $6.2 \pm 0.5 \times 10^4$ ats/$g_{(Qz)}$ that is preserved in mostly fine-grained (< 500 μm) sediment. This mean nuclide concentration does not contain buried sediment signatures, because we found that some active rivers contain old, partly shielded material from floodplain burial. These burial signatures were identified by ^{26}Al/^{10}Be ratios being lower than

what we would expect for surfaces under continuous irradiation of cosmic rays. Our burial-free nuclide concentration does not deviate much from that of the Andean source area (flux-weighted mean of $5.2 \pm 0.5 \times 10^4$ ats/$g_{(Qz)}$).

The nuclide concentration detected in fine-grained, nonburied sediment in the central Amazonian rivers is representative of Andean denudation and is not affected by storage within the large Amazon floodplain. We can thus provide an independent meter of sediment production in the world's largest depositional basin. The calculated sediment flux passing Óbidos amounts to 610 Mt/yr from our cosmogenic nuclide-derived denudation rates. Despite pronounced differences in integration time scales, our estimate compares reasonably well to an average total recent load of ~1000 Mt/yr from published gauging and dissolved load records and to a sediment discharge estimate of 550–1030 Mt/yr from ^{210}Pb activity profiles in the Amazon delta, which integrates over the past 1000 years. It is the ability of the large Amazon floodplain to buffer against changes in erosion in the source areas that controls the stability of sediment output fluxes for the Amazon River basin.

ACKNOWLEDGMENTS

We are most thankful to Jérôme Gaillardet for help with initiating this project and discussions. Great thanks also go to Jane K. Willenbring and Julien Bouchez, who helped to clarify and sharpen the focus of this manuscript. Edgardo Latrubesse is acknowledged for discussions, and we would like to thank Patricia Moreira-Turcq, Patrick Seyler, and the boat crew of the *Commandante Cuadros* for support during the 2006 field campaign. We thank Frédérique Seyler for sampling the Branco River and Manuela Dziggel for crafting Figure 2. Eduardo Garzanti, one anonymous reviewer, and Associate Editor Massimo Mattei are thanked for their productive and helpful comments on this manuscript. This work was supported by Deutsche Forschungsgemeinschaft grant Bl 562/2-2.

REFERENCES CITED

Abbott, M.B., Wolfe, B.B., Wolfe, A.P., Seltzer, G.O., Aravena, R., Mark, B.G., Polissar, P.J., Rodbell, D.T., Rowe, H.D., and Vuille, M., 2003, Holocene paleohydrology and glacial history of the central Andes using multiproxy lake sediment studies: Palaeogeography, Palaeoclimatology, Palaeoecology, v. 194, no. 1–3, p. 123–138, doi: 10.1016/S0031-0182(03)00274-8.

Balco, G., Stone, J.O.H., and Jennings, C., 2005, Dating Plio-Pleistocene glacial sediments using the cosmic-ray-produced radionuclides ^{10}Be and ^{26}Al: American Journal of Science, v. 305, no. 1, p. 1–41, doi: 10.2475/ajs.305.1.1.

Barnes, J.B., Ehlers, T.A., McQuarrie, N., O'Sullivan, P.B., and Tawackoli, S., 2008, Thermochronometer record of central Andean plateau growth, Bolivia (19.5° S): Tectonics, v. 27, no. 3, TC3003, doi: 10.1029/2007TC002174.

Benjamin, M.T., Johnson, N.M., and Naeser, C.W., 1987, Recent rapid uplift in the Bolivian Andes: Evidence from fission-track dating: Geology, v. 15, no. 7, p. 680–683, doi: 10.1130/0091-7613(1987)15<680:RRUITB>2.0.CO;2.

Bierman, P., and Steig, E.J., 1996, Estimating rates of denudation using cosmogenic isotope abundances in sediment: Earth Surface Processes and Landforms, v. 21, no. 2, p. 125–139, doi: 10.1002/(SICI)1096-9837(199602)21:2<125::AID-ESP511>3.0.CO;2-8.

Borradaile, G., 2003, Statistics of Earth Science Data—Their distribution in time, space and orientation: Berlin, Springer Verlag, 351 p.

Caputo, M.V., 1991, Solimoes megashear: Intraplate tectonics in northwestern Brazil: Geology, v. 19, no. 3, p. 246–249, doi: 10.1130/0091-7613(1991)019<0246:SEMITI>2.3.CO;2.

Chmeleff, J., von Blanckenburg, F., Kossert, K., and Jakob, D., 2010, Determination of the ^{10}Be half-life by multi-collector ICP-MS and liquid scintillation counting: Nuclear Instruments and Methods in Physics Research, Section B, Beam Interactions with Materials and Atoms, v. 268, no. 2, p. 192–199, doi: 10.1016/j.nimb.2009.09.012.

Coynel, A., Schäfer, J., Hurtrez, J.-E., Dumas, J., Etcheber, H., and Blanc, G., 2004, Sampling frequency and accuracy of SPM flux estimates in two contrasted drainage basins: The Science of the Total Environment, v. 330, no. 1–3, p. 233–247.

Cross, S.L., Baker, P.A., Seltzer, G.O., Fritz, S.C., and Dunbar, R.B., 2000, A new estimate of the Holocene lowstand level of Lake Titicaca, central Andes, and implications for tropical palaeohydrology: The Holocene, v. 10, no. 1, p. 21–32, doi: 10.1191/095968300671452546.

Dosseto, A., Bourdon, B., Gaillardet, J., Allegre, C.J., and Filizola, N., 2006a, Time scale and conditions of weathering under tropical climate: Study of the Amazon basin with U-series: Geochimica et Cosmochimica Acta, v. 70, no. 1, p. 71–89, doi: 10.1016/j.gca.2005.06.033.

Dosseto, A., Bourdon, B., Gaillardet, J., Maurice-Bourgoin, L., and Allegre, C.J., 2006b, Weathering and transport of sediments in the Bolivian Andes: Time constraints from uranium-series isotopes: Earth and Planetary Science Letters, v. 248, no. 3–4, p. 759–771, doi: 10.1016/j.epsl.2006.06.027.

Dunne, T., Mertes, L.A.K., Meade, R.H., Richey, J.E., and Forsberg, B.R., 1998, Exchanges of sediment between the flood plain and channel of the Amazon River in Brazil: Geological Society of America Bulletin, v. 110, no. 4, p. 450–467, doi: 10.1130/0016-7606(1998)110<0450:EOSBTF>2.3.CO;2.

Filizola, N., 2003, Transfer sédimentaire actuel par les fleuves amazoniens [Ph.D. thesis]: France, Université de Toulouse III, 292 p.

Filizola, N., and Guyot, J.L., 2009, Suspended sediment yields in the Amazon basin: An assessment using the Brazilian national data set: Hydrological Processes, v. 23, p. 3207–3215, doi: 10.1002/hyp.7394.

Franzinelli, E., and Igreja, H., 2002, Modern sedimentation in the Lower Negro River, Amazonas State, Brazil: Geomorphology, v. 44, no. 3–4, p. 259–271.

Franzinelli, E., and Potter, P.E., 1983, Petrology, chemistry, and texture of modern river sands, Amazon river system: The Journal of Geology, v. 91, no. 1, p. 23–39, doi: 10.1086/628742.

Gaillardet, J., Dupre, B., Allegre, C.J., and Negrel, P., 1997, Chemical and physical denudation in the Amazon River basin: Chemical Geology, v. 142, no. 3–4, p. 141–173, doi: 10.1016/S0009-2541(97)00074-0.

Gibbs, R.J., 1967, Amazon River—Environmental factors that control its dissolved and suspended load: Science, v. 156, no. 3783, p. 1734–1737, doi: 10.1126/science.156.3783.1734.

Goethals, M.M., Hetzel, R., Niedermann, S., Wittmann, H., Fenton, C.R., Kubik, P., Christl, M., and Von Blanckenburg, F., 2009, An improved experimental determination of cosmogenic ^{10}Be/^{21}Ne and ^{26}Al/^{21}Ne production ratios in quartz: Earth and Planetary Science Letters, v. 284, p. 187–198, doi: 10.1016/j.epsl.2009.04.027.

Granger, D.E., 2006, A review of burial dating methods using 26Al and 10Be, *in* Siame, L., et al., eds., In Situ–Produced Cosmogenic Nuclides and Quantification of Geological Processes: Geological Society of America Special Paper 415, p. 1–16, doi: 10.1130/2006.2415(01).

Granger, D.E., and Muzikar, P.F., 2001, Dating sediment burial with in situ-produced cosmogenic nuclides: Theory, techniques, and limitations: Earth and Planetary Science Letters, v. 188, no. 1–2, p. 269–281, doi: 10.1016/S0012-821X(01)00309-0.

Granger, D.E., and Riebe, C.S., 2007, Cosmogenic nuclides in weathering and erosion, *in* Drever, J.I., ed., Treatise on Geochemistry: Surface and Ground Water, Weathering, and Soils: London, Elsevier.

Granger, D.E., Kirchner, J.W., and Finkel, R., 1996, Spatially averaged long-term erosion rates measured from in situ-produced cosmogenic nuclides in alluvial sediment: The Journal of Geology, v. 104, no. 3, p. 249–257, doi: 10.1086/629823.

Guyot, J.L., Jouanneau, J.M., Quintanilla, J., and Wasson, J.G., 1993, Dissolved and suspended sediment loads exported from the Andes by the Beni River (Bolivian Amazonia) during a flood: Geodinamica Acta, v. 6, no. 4, p. 233–241.

Guyot, J.L., Filizola, N., Quintanilla, J., and Cortez, J., 1996, Dissolved solids and suspended sediment yields in the Rio Madeira basin, from the Bolivian Andes to the Amazon: Exeter, UK, Proceedings of the Exeter Symposium, p. 55–63.

Guyot, J.L., Jouanneau, J.M., and Wasson, J.G., 1999, Characterization of river bed and suspended sediments in the Rio Madeira drainage basin (Bolivian Amazonia): Journal of South American Earth Sciences, v. 12, no. 4, p. 401–410, doi: 10.1016/S0895-9811(99)00030-9.

Guyot, J.L., Filizola, N., and Laraque, A., 2005, The suspended sediment flux of the River Amazon at Óbidos, Brazil, 1995–2003: Foz do Iguaco, Brazil, Proceedings of Symposium S1 held during the Seventh International Association of Hydrological Sciences Scientific Assembly, p. 347–354.

Guyot, J.L., Bazan, H., Fraizy, P., Ordonez, J.J., Armijos, E., and Laraque, A., 2007a, Suspended sediment yields in the Amazon basin of Peru: A first estimation: Perugia, Italy, Water Quality and Sediment Behaviour of the Future, p. 3–10.

Guyot, J.L., Jouanneau, J.M., Soares, L., Boaventura, G., Maillet, N., and Lagane, C., 2007b, Clay mineral composition of river sediments in the Amazon Basin: Catena, v. 71, p. 340–356, doi: 10.1016/j.catena.2007.02.002.

Hartmann, L.A., and Delgado, I.D., 2001, Cratons and orogenic belts of the Brazilian Shield and their contained gold deposits: Mineralium Deposita, v. 36, no. 3–4, p. 207–217, doi: 10.1007/s001260100175.

Hofmann, H.J., Beer, J., Bonani, G., Vongunten, H.R., Raman, S., Suter, M., Walker, R.L., Wolfli, W., and Zimmermann, D., 1987, ^{10}Be: Half-life and AMS-standards: Nuclear Instruments and Methods in Physics Research, Section B, Beam Interactions with Materials and Atoms, v. 29, no. 1–2, p. 32–36, doi: 10.1016/0168-583X(87)90198-4.

Irion, G., Muller, J., deMello, J.N., and Junk, W.J., 1995, Quaternary geology of the Amazonian lowland: Geo-Marine Letters, v. 15, no. 3–4, p. 172–178, doi: 10.1007/BF01204460.

Irion, G., Bush, M.B., de Mello, J.A.N., Stuben, D., Neumann, T., Muller, G., De, J.O., and Junk, J.W., 2006, A multiproxy palaeoecological record of Holocene lake sediments from the Rio Tapajos, eastern Amazonia: Palaeogeography, Palaeoclimatology, Palaeoecology, v. 240, no. 3–4, p. 523–535, doi: 10.1016/j.palaeo.2006.03.005.

Irion, G., Müller, J., Morais, J.O., Keim, G., de Mello, J.N., and Junk, W.J., 2009, The impact of Quaternary sea level changes on the evolution of the Amazonian lowland: Hydrological Processes, v. 23, no. 22, p. 3168–3172, doi: 10.1002/hyp.7386.

Jerolmack, D. J., and Sadler, P., 2007, Transience and persistence in the depositional record of continental margins: Journal of Geophysical Research-Earth Surface, v. 112, no. F3.

Johnsson, M.J., and Meade, R.H., 1990, Chemical weathering of fluvial sediments during alluvial storage—The Macuapanim island point-bar, Solimoes River, Brazil: Journal of Sedimentary Petrology, v. 60, no. 6, p. 827–842.

Kubik, P.W., Ivy-Ochs, S., Masarik, J., Frank, M., and Schluchter, C., 1998, ^{10}Be and ^{26}Al production rates deduced from an instantaneous event within the dendro-calibration curve, the landslide of Kofels, Otz Valley, Austria: Earth and Planetary Science Letters, v. 161, no. 1–4, p. 231–241, doi: 10.1016/S0012-821X(98)00153-8.

Kuehl, S.A., Demaster, D.J., and Nittrouer, C.A., 1986, Nature of sediment accumulation on the Amazon continental-shelf: Continental Shelf Research, v. 6, no. 1–2, p. 209–225, doi: 10.1016/0278-4343(86)90061-0.

Langbein, W., and Schumm, S.A., 1958, Yield of sediment in relation to mean annual precipitation: Transactions, American Geophysical Union, v. 39, p. 1076–1084.

Laraque, A., Filizola, N., and Guyot, J.L., 2005, The spatial and temporal variability of sediment transport in the Brazilian Amazon basin, based on a regular 10-day sampling programme: Foz do Iguaco, Brazil, Proceedings of symposium S1 held during the Seventh International Association of Hydrological Sciences Scientific Assembly, p. 250–258.

Laraque, A., Bernal, C., Bourrel, L., Darrozes, J., Christophoul, F., Armijos, E., Fraizy, P., Pombosa, R., and Guyot, J.L., 2009, Sediment budget of the Napo River, Amazon basin, Ecuador and Peru: Hydrological Processes, v. 23, no. 25, p. 3509–3524, doi: 10.1002/hyp.7463.

Latrubesse, E.M., and Franzinelli, E., 2005, The late Quaternary evolution of the Negro River, Amazon, Brazil: Implications for island and floodplain formation in large anabranching tropical systems: Geomorphology, v. 70, no. 3–4, p. 372–397, doi: 10.1016/j.geomorph.2005.02.014.

Martinez, J.-M., and Le Toan, T., 2007, Mapping of flood dynamics and spatial distribution of vegetation in the Amazon floodplain using multitemporal SAR data: Remote Sensing of Environment, v. 108, no. 3, p. 209–223, doi: 10.1016/j.rse.2006.11.012.

Martinez, J.M., Guyot, J.L., Filizola, N., and Sondag, F., 2009, Increase in suspended sediment discharge of the Amazon River assessed by monitoring network and satellite data: Catena, v. 79, no. 3, p. 257–264, doi: 10.1016/j.catena.2009.05.011.

Masarik, J., Frank, M., Schafer, J.M., and Wieler, R., 2001, Correction of in situ cosmogenic nuclide production rates for geomagnetic field intensity variations during the past 800,000 years: Geochimica et Cosmochimica Acta, v. 65, no. 17, p. 2995–3003, doi: 10.1016/S0016-7037(01)00652-4.

Mathieu, D., Bernat, M., and Nahon, D., 1995, Short-lived U and Th isotope distribution in a tropical laterite derived from granite (Pitinga river basin, Amazonia, Brazil): Application to assessment of weathering rate: Earth and Planetary Science Letters, v. 136, no. 3–4, p. 703–714, doi: 10.1016/0012-821X(95)00199-M.

Maurice-Bourgoin, L., Aalto, R., and Guyot, J., 2002, Sediment-associated mercury distribution within a major Amazon tributary: Century-scale contamination history and importance of flood plain accumulation: Alice Springs, Australia, Structure, Function and Management Implications of Fluvial Sedimentary Systems International Symposium, September 2002, p. 161–168.

Maurice-Bourgoin, L., Bonnet, M.P., Martinez, J.M., Kosuth, P., Cochonneau, G., Moreira-Turcq, P., Guyot, J.L., Vauchel, P., Filizola, N., and Seyler, P., 2007, Temporal dynamics of water and sediment exchanges between the Curuaí floodplain and the Amazon River, Brazil: Amsterdam, Journal of Hydrology, v. 335, no. 1–2, p. 140–156, doi: 10.1016/j.jhydrol.2006.11.023.

Meade, R.H., 1985, Suspended Sediment in the Amazon River and its tributaries in Brazil during 1982–1984: U.S. Geological Survey Open-File Report 85-492, p. 1–39.

Meade, R.H., Nordin, C.F., Curtis, W.F., Mahoney, H.A., and Delaney, B.M., 1979, Suspended sediment and velocity data, Amazon River and tributaries, June–July 1976 and May–June 1977: U.S. Geological Survey Open-File Report 79-515, p. 1–42.

Meade, R.H., Dunne, T., Richey, J.E., Santos, U., and Salati, E., 1985, Storage and remobilization of suspended sediment in the lower Amazon River of Brazil: Science, v. 228, p. 488–490, doi: 10.1126/science.228.4698.488.

Mertes, L.A.K., and Dunne, T., 2007, Effects of tectonism, climate change, sea-level change on the form and behaviour of the Amazon River and its floodplain, *in* Gupta, A., ed., Large Rivers: Geomorphology and Management: New York, John Wiley and Sons, p. 115–144.

Mertes, L.A.K., and Meade, R.H., 1985, Particle sizes of sands collected from the bed of the Amazon River and its tributaries during 1982–1984: U.S. Geological Survey Open-File Report 85-333, p. 1–16.

Mertes, L.A.K., Dunne, T., and Martinelli, L.A., 1996, Channel-floodplain geomorphology along the Solimoes-Amazon River, Brazil: Geological Society of America Bulletin, v. 108, no. 9, p. 1089–1107, doi: 10.1130/0016-7606(1996)108<1089:CFGATS>2.3.CO;2.

Métivier, F., 1999, Diffusive-like buffering and saturation of large rivers: Physical Review E: Statistical Physics, Plasmas, Fluids, and Related Interdisciplinary Topics, v. 60, no. 5, p. 5827–5832.

Métivier, F., and Gaudemer, Y., 1999, Stability of output fluxes of large rivers in South and East Asia during the last 2 million years: Implications on floodplain processes: Basin Research, v. 11, no. 4, p. 293–303, doi: 10.1046/j.1365-2117.1999.00101.x.

Moreira-Turcq, P., Seyler, P., Guyot, J.L., and Etcheber, H., 2003, Exportation of organic carbon from the Amazon River and its main tributaries: Hydrological Processes, v. 17, p. 1329–1344, doi: 10.1002/hyp.1287.

Nittrouer, C.A., and Kuehl, S.A., 1995, Geological significance of sediment transport and accumulation on the Amazon continental shelf—Preface: Marine Geology, v. 125, no. 3–4, p. 175–176, doi: 10.1016/0025-3227(95)00073-8.

Nordin, C.F., Meade, R.H., Curtis, W.F., Bosio, N.J., and Landim, P.M.B., 1980, Size distribution of Amazon River bed sediment: Nature, v. 286, no. 5768, p. 52–53, doi: 10.1038/286052a0.

Phillips, J.D., 2003, Alluvial storage and the long-term stability of sediment yields: Basin Research, v. 15, no. 2, p. 153–163, doi: 10.1046/j.1365-2117.2003.00204.x.

Phillips, J.D., and Slattery, M.C., 2006, Sediment storage, sea level, and sediment delivery to the ocean by coastal plain rivers: Progress in Physical Geography, v. 30, no. 4, p. 513–530, doi: 10.1191/0309133306pp494ra.

Potter, P.E., 1994, Modern sands of South America: Composition, provenance and global significance: Geologische Rundschau, v. 83, p. 212–232, doi: 10.1007/BF00211904.

Rossetti, D.D., de Toledo, P.M., and Goes, A.M., 2005, New geological framework for Western Amazonia (Brazil) and implications for biogeography and evolution: Quaternary Research, v. 63, no. 1, p. 78–89, doi: 10.1016/j.yqres.2004.10.001.

Safran, E.B., Blythe, A., and Dunne, T., 2006, Spatially variable exhumation rates in orogenic belts: An Andean example: The Journal of Geology, v. 114, no. 6, p. 665–681, doi: 10.1086/507613.

Schaller, M., von Blanckenburg, F., Hovius, N., and Kubik, P.W., 2001, Large-scale erosion rates from in situ-produced cosmogenic nuclides in European river sediments: Earth and Planetary Science Letters, v. 188, no. 3–4, p. 441–458, doi: 10.1016/S0012-821X(01)00320-X.

Seyler, P.T., and Boaventura, G., 2003, Distribution and partition of trace metals in the Amazon basin: Hydrological Processes, v. 17, p. 1345–1361, doi: 10.1002/hyp.1288.

Stallard, R.F., 1995, Tectonic, environmental, and human aspects of weathering and erosion—A global review using a steady-state perspective: Annual Review of Earth and Planetary Sciences, v. 23, p. 11–39, doi: 10.1146/annurev.ea.23.050195.000303.

Strasser, M., 2002, Estudo da geometria das formas de fundo no curso médio do Rio Amazonas [M.S. thesis]: Universidade Federal do Rio de Janeiro, 100 p.

Synal, H.A., Bonani, G., Dobeli, M., Ender, R.M., Gartenmann, P., Kubik, P.W., Schnabel, C., and Suter, M., 1997, Status report of the PSI/ETH AMS facility: Nuclear Instruments and Methods in Physics Research, Section B, Beam Interactions with Materials and Atoms, v. 123, no. 1–4, p. 62–68, doi: 10.1016/S0168-583X(96)00608-8.

van der Hammen, T., and Hooghiemstra, H., 2000, Neogene and Quaternary history of vegetation, climate, and plant diversity in Amazonia: Quaternary Science Reviews, v. 19, no. 8, p. 725–742, doi: 10.1016/S0277-3791(99)00024-4.

Vital, H., Stattegger, K., and Garbe-Schoenberg, C.-D., 1999, Composition and trace-element geochemistry of detrital clay and heavy-mineral suites of the lowermost Amazon River: A provenance study: Journal of Sedimentary Research, v. 69, no. 3, p. 563–575.

von Blanckenburg, F., 2005, The control mechanisms of erosion and weathering at basin scale from cosmogenic nuclides in river sediment: Earth and Planetary Science Letters, v. 237, no. 3–4, p. 462–479.

von Blanckenburg, F., Hewawasam, T., and Kubik, P. W., 2004, Cosmogenic nuclide evidence for low weathering and denudation in the wet, tropical highlands of Sri Lanka: Journal of Geophysical Research-Earth Surface, v. 109, no. F3.

Walling, D.E., 1983, The sediment delivery problem: Amsterdam, Journal of Hydrology, v. 65, no. 1–3, p. 209–237, doi: 10.1016/0022-1694(83)90217-2.

Walling, D.E., and Webb, B., 1981, The reliability of suspended sediment load data: Erosion and Sediment Transport Measurement: Florence, Italy, International Association of Hydrological Sciences Publication, v. 113, p. 177–194.

Wittmann, H., 2008, New applications to in situ-produced cosmogenic nuclides in river sediment: High mountain belt denudation in the Swiss Alps and Bolivian Andes and sediment transfer and storage in the Amazon basin [Ph.D. thesis]: University of Hannover, 178 p.

Wittmann, H., and von Blanckenburg, F., 2009, Cosmogenic nuclide budgeting of floodplain sediment transfer: Geomorphology, v. 109, no. 3–4, p. 246–256, doi: 10.1016/j.geomorph.2009.03.006.

Wittmann, H., von Blanckenburg, F., Kruesmann, T., Norton, K.P., and Kubik, P.W., 2007, Relation between rock uplift and denudation from cosmogenic nuclides in river sediment in the central Alps of Switzerland: Journal of Geophysical Research-Earth Surface, v. 112, no. F4.

Wittmann, H., von Blanckenburg, F., Guyot, J.L., Maurice, L., and Kubik, P.W., 2009, From source to sink: Preserving the cosmogenic ^{10}Be-derived denudation rate signal of the Bolivian Andes in sediment of the Beni and Mamoré foreland basins: Earth and Planetary Science Letters, v. 288, no. 3–4, p. 463–474, doi: 10.1016/j.epsl.2009.10.008.

Manuscript Received 19 April 2010
Revised Manuscript Received 2 August 2010
Manuscript Accepted 6 August 2010

Printed in the USA